A Quadratic Programming Formulation for the Solution of Layered Elastic Contact Problems: Example Applications and Experimental Validation

S. Reina, D. Dini, D.A. Hills, Y. Iida

Accepted Manuscript

Title: A Quadratic Programming Formulation for the Solution of Layered Elastic Contact Problems: Example Applications and Experimental Validation

Authors: S. Reina, D. Dini, D.A. Hills, Y. Iida

PII: S0997-7538(10)00141-5

DOI: 10.1016/j.euromechsol.2010.12.003

Reference: EJMSOL 2658

To appear in: *European Journal of Mechanics / A Solids*

Received Date: 10 June 2010

Revised Date: 6 December 2010

Accepted Date: 10 December 2010

Please cite this article as: Reina, S., Dini, D., Hills, D.A., Iida, Y. A Quadratic Programming Formulation for the Solution of Layered Elastic Contact Problems: Example Applications and Experimental Validation, European Journal of Mechanics / A Solids (2010), doi: 10.1016/j.euromechsol.2010.12.003

A Quadratic Programming Formulation for the Solution of Layered Elastic Contact Problems: Example Applications and Experimental Validation

S. Reina[a], D. Dini[a,1], D. A. Hills[b], and Y. Iida[a]

[a]Department of Mechanical Engineering,
Imperial College London, South Kensington Campus, Exhibition Road,
London SW7 2AZ, UK.
[b]Department of Engineering Science,
University of Oxford, Parks Road,
Oxford OX1 3PJ, UK.

Abstract

The development of a quadratic programming formulation for the solution of layered elastic contact problems in the presence of friction is presented in this paper. Conveyor belts, tyred wheels, composite cylinders, and conrod bearings, are classical examples of systems which can be studied using the efficient numerical methodology proposed here. In this type of mechanical assembly, micro-slip between the mating surfaces often occurs and may eventually lead to system failure. Accurately capturing the evolution of slip and stick areas using a computationally inexpensive procedure (as an alternative to full finite element analysis) is therefore key to preventing these failures and to improving the design of various engineering components.
The proposed approach is first tested and validated against classical marching-in-time solutions for two-dimensional layered systems in the presence of both static and moving loads. Results are then extended to demonstrate the feasibility of the technique to study systems with multiple slip regions and to solve rolling contact problems of practical interest. Finally, the numerical methodology is successfully applied to the prediction of frictional creep of tyred cylinders. Experimental corroboration has been obtained by testing tyred discs.

Keywords: Layered Systems, Rolling Contact, Integral Transforms, Quadratic Programming, Frictional Creep.

[1] Corresponding Author: Tel. +44(0)2075947242; Fax: +44(0)2075947023; Email address: d.dini@imperial.ac.uk.

1 Notation

Notation

2 Introduction

Components which are notionally in stationary contact, but subjected to cyclic or vibratory loads often do not exhibit complete adhesion, and may be susceptible to some slip over at least part of the contact [1]. This is likely to lead to degradation of the surfaces [2], but it may be a transitory phenomenon; the coefficient of friction may gradually increase as surface modification proceeds [3], or residual interfacial shearing tractions may develop, leading to frictional shakedown [4]. On the other hand, slip may continue indefinitely. If it does, then, there are two possible responses: (1) in each cycle the total net slip may be zero, so that there is no rigid body movement , or 'creep', and the resulting behaviour is analogous to cyclic plasticity whilst (2) in other cases there may be a net movement, and creep ensues, *cf.* ratchetting. It is very important to be able to determine into which class a given problem falls. This has led to detailed investigations of the possibility of extending the elastic shakedown theorem to frictional shakedown problems. One output of these studies is that, although Melan's theorem may profitably be used for frictional systems, it applies only to 'uncoupled' systems where the direct tractions are unaffected by relative tangential displacement between the surfaces in contact [4].

In general, continuing slip may lead to system failure [5]. For example, engine connecting rods suffer severe damage if the bushes slip with respect to the housing [6], and may exhibit continuous rotation. Classic approaches to the design of these assemblies are based on macroscopic criteria, such as localised yielding. Also, interfacial micro-slip is not easily captured using standard numerical design tools, especially if the loading history is complicated, and where simultaneous slip may occur at different locations along the mating surfaces [7]. Finite element or boundary element approaches *may* be able to provide accurate results, but they often face limitations in terms of both computational time and solution convergence when applied to the solution of complex partial slip contact problems under cyclic loading [8].

Turning, now, to shrink-fitted and/or layered systems, a semi-analytical procedure, normally

referred to as the distributed dislocation technique, has been successfully used to analyse microslip in layered frictional contact problems [9-14]. The applicability of this methodology has been recently extended by the authors to layered cylinders undergoing rolling contact [15]. The principal limitation is that, if the classical integral equation procedure is adopted, it is extremely difficult to determine the locations of the stick/slip transition points systematically and, if there are several such points, long-winded iterative schemes may be needed [8]. In the approach advocated here, the advantages of the dislocation kernel (which maintains remote boundary conditions) is retained but the problems of the integral equation are averted by formulating the contact problem in terms of a 'quadratic cost function' to be minimised [21]. The problem can therefore be solved using quadratic programming. Building on the capabilities of linear programming to be applied to tackle contact problems (*e.g.* see Kalker [17] [18]), this optimisation technique has been widely applied in mechanics to solve problems with both linear or non-linear constraints. Its applicability to two and three dimensional elastic contact problems has been demonstrated in the '80s [19] [20]. Nowell and Dai [21] also used quadratic programming to solve the fretting configuration. The technique is well established in other fields of applied mechanics; for example, in the late '60s, Maier had already demonstrated its effectiveness in solving non-linear structural problems [22], elastic-perfectly plastic structures [23] and problems involving creep [24]. Finally, quadratic programming has been applied in combination either with finite element methods (FEM) [26] [27], or boundary element methods (BEM) [25] to investigate problems related to fracture and contact mechanics.

In this paper we formulate, for the first time, the problem of a layered system, mounted on a (rigid or elastic) substrate in the presence of friction and subjected to loading conditions giving rise to micro-slip or creep, using the distributed dislocation technique, within the quadratic programming framework. We then demonstrate its use for the solution of rolling contact problems for layered systems. The development of an experimental technique to measure the extent of creep in layered rolling contact problems is also presented. A preliminary comparison between numerical and experimental results is performed to confirm the validity of the proposed numerical technique.

3 Formulation

3.1 Stationary loads

Figure 1 shows schematically an elastic layer under transverse plane strain, pressed against a substrate in the presence of friction and subjected to external normal and tangential loading. This problem may be seen as a generalisation of the contact problem extensively discussed in [15].

Figure 1

The coordinate origin is positioned at the interface between the layer and the substrate, and the Coulomb-Amontons friction law is adopted so that the coefficient of friction is independent of slip-velocity. The solution to the 'bilateral' problem (where coefficient of friction sufficiently high to prevent all slip) is found first, and denoted by $\sigma_{xy}^{bil}(x)$, $\sigma_{yy}^{bil}(x)$ for shear and direct tractions, respectively. Slip along the interface is subsequently introduced by distributing dislocations within the slip region(s), and the corrective solution denoted by $\sigma_{xy}^{corr}(x)$ and $\sigma_{yy}^{corr}(x)$ for shear and direct tractions, respectively. The total tractions are then given by:

$$\begin{bmatrix}\sigma_{yy}(x,0)\\ \sigma_{xy}(x,0)\end{bmatrix} = \begin{bmatrix}\sigma_{yy}^{bil}(x)\\ \sigma_{xy}^{bil}(x)\end{bmatrix} + \begin{bmatrix}\sigma_{yy}^{corr}(x)\\ \sigma_{xy}^{corr}(x)\end{bmatrix}, \tag{1}$$

where the corrective terms are:

$$\begin{bmatrix}\sigma_{yy}^{corr}(x)\\ \sigma_{xy}^{corr}(x)\end{bmatrix} = A_{SM,DM}\int_{-\infty}^{+\infty} B_x(\xi)\begin{bmatrix}G_{yy}(x,\xi)\\ G_{xy}(x,\xi)\end{bmatrix}d\xi, \tag{2}$$

A is the contact compliance, the subscripts SM and DM refer, respectively, to similar ($E_1 = E_2$ and $\nu_1 = \nu_2$) and dissimilar ($E_1 \neq E_2$ and/or $\nu_1 \neq \nu_2$) material pairs, $B_x(\xi)$ is the dislocation density, and $G_{yy}(x,\xi)$ and $G_{xy}(x,\xi)$ are the influence functions associated with the glide dislocations (see Appendix A). Separation between the layer and the substrate is not considered.

The interface conditions are now defined. Where the frictional law is not violated, stick occurs and this means that:

$$h(x) = 0 \tag{3}$$

$$|\sigma_{xy}(x,0)| \leq -f\sigma_{yy}(x,0), \tag{4}$$

where $h(x)$ is the the relative displacement between the bodies in contact defined by:

$$h(x) = u_{layer}(x) - u_{substrate}(x) \tag{5}$$

and $u_{layer}(x)$ and $u_{substrate}(x)$ represent, respectively, the upper body and the lower body surface tangential displacement. Where the friction law is violated, slip displacement takes place and:

$$|\sigma_{xy}(x,0)| = f\,|\sigma_{yy}(x,0)| \tag{6}$$

whilst the sign of the shear is dictated by the requirement that it opposes slip, so that:

$$sgn(\sigma_{xy}(x,0)) = sgn\left(\dot{h}(x)\right). \tag{7}$$

Here, the sign of the relative slip and its first derivative in time coincide [11]:

$$sgn\left(\dot{h}(x)\right) = sgn(h(x)) \tag{8}$$

so that the final expression for shear traction in the presence of slip is:

$$\sigma_{xy}(x,0) = -f\sigma_{yy}(x,0)\frac{h(x)}{|h(x)|}. \tag{9}$$

Lastly, uniqueness demands that:

$$\int_{-\infty}^{+\infty} B_x(\xi)\,d\xi = 0 \tag{10}$$

although, of course, the integrand is zero except in the slip regions.

The classic way of solving the problem requires guessing the location and extent of each slip area present and iterating the solution until (10) is satisfied, but this can easily become very cumbersome. The formulation developed below relies on the use of optimisation strategies to avoid this.

If both sides of the equation for slip (9) are multiplied by $h(x)$, we obtain:

$$\sigma_{xy}(x,0)\,h(x) + f\sigma_{yy}(x,0)\,|h(x)| = 0. \tag{11}$$

It should be noted that this also applies where stick occurs. Thus, the above boundary condition is valid along the whole interface, with no distinction made between stick and slip areas. If we now integrate (11) along the entire interface, we can define the functional of our layered elastic

problem, $\tilde{F}$, as follows:

$$\tilde{F} = \int_{-\infty}^{+\infty} \left\{ - \left[\sigma_{xy}\left(x,0\right) h\left(x\right) + f \sigma_{yy}\left(x,0\right) \left| h\left(x\right) \right| \right] \right\} dx \tag{12}$$

The minus sign was added in front of the integrand as this makes it always positive. This property can be easily proved, because

$$-\sigma_{xy}\left(x,0\right) h\left(x\right) - f\sigma_{yy}\left(x,0\right) \left| h\left(x\right) \right| \geq - \left| \sigma_{xy}\left(x,0\right) \right| \left| h\left(x\right) \right| - f\sigma_{yy}\left(x,0\right) \left| h\left(x\right) \right| \geq 0 \tag{13}$$

where the first inequality becomes an equality if and only if slip vanishes or traction has the same sign direction as slip, whilst the second inequality turns into an equality if and only if the shear tractions are f times $\sigma_{yy}\left(x,0\right)$ or slip vanishes. Now, if the solution to the layer problem is substituted in (12), the functional goes to zero. On the other hand, if any other combination of pressure, tangential tractions and displacement is used, the value of the functional is strictly positive. We conclude that the solution to the problem may be found by minimising the value of the functional, taking into account the frictional law adopted together with the condition for uniqueness of the elastic solution [17]. We now focus our attention on how the functional and boundary conditions can be discretised.

3.1.1 Discretisation and Numerical Integration

The integral representing the functional is improper as the integration domain is unbounded. However, the integration interval may be truncated as no slip is permitted as x goes to $\pm\infty$. The interval of integration may therefore be reduced until it just includes all slip areas. In order to compute the value of (12), we assume that traction and displacement fields are sampled at a finite number of equally spaced points, indicated with the letter j, with $j = 1..n_p$. The distance between the equally spaced points is indicated with the letter d_{sup}. Thus, the integration in (12) can be replaced by a summation and, consequently, the functional rewritten as follows:

$$\tilde{F} = - \sum_{j=1}^{n_p} \left[\left(\sigma_{xy,j}^{bil} + \sigma_{xy,j}^{corr} \right) h_j + f \left(\sigma_{yy,j}^{bil} + \sigma_{yy,j}^{corr} \right) \left| h_j \right| \right] d_{\text{sup}}. \tag{14}$$

The presence of the absolute value of the relative displacement, $h\left(x\right)$, complicates the formulation. A similar problem was first faced and solved by Kalker [17] who proposed that the absolute value could be replaced by the sum of two positive quantities, and the term within the

sign of absolute value by the difference between the same quantities. This transformation is applied by replacing the displacement term, h_j, and its absolute values, $|h_j|$, as follows:

$$h_j = h'_j - h''_j \tag{15}$$

$$|h_j| = h'_j + h''_j \tag{16}$$

where h'_j are h''_j are positive quantities such that if $h_j > 0$, $h_j = h'_j$ and $h''_j = 0$, whereas if $h_j < 0$, $h_j = -h''_j$ and $h'_j = 0$, and therefore the product $h'_j h''_j$ is always zero. This constitutes a set of complementary variables and they are the independent variables to be determined by performing the minimisation of the functional (14) using algorithms conventionally employed to solve Linear Complementarity Problems (LCP).

The final discretised form of the functional is

$$\tilde{F} = -\sum_{j=1}^{n_p} \left[\left(\sigma^{bil}_{xy,j} + \sigma^{corr}_{xy,j} \right) \left(h'_j - h''_j \right) + f \left(\sigma^{bil}_{yy,j} + \sigma^{corr}_{yy,j} \right) \left(h'_j + h''_j \right) \right] d_{\text{sup}}. \tag{17}$$

We now focus our attention on the corrective terms. The dislocation density is related to the slip displacement by:

$$B_x(\xi) = -\frac{dh(\xi)}{dx}. \tag{18}$$

The gradient of the slip displacement may be calculated using the finite difference method. The position of a generic midpoint coordinate, k, where the dislocation density is sampled can be expressed as follows:

$$x_k = \frac{x_j}{2} + \frac{x_{j+1}}{2} \tag{19}$$

and the discretised form of (18) is therefore

$$B_{x_k} = -\frac{h_{j+1} - h_j}{x_{j+1} - x_j} = \frac{h_j - h_{j+1}}{d_{\text{sup}}}. \tag{20}$$

The integral in (2) is discretised by representing the dislocation density function using overlapping triangles [31], which provide a piecewise linear approximation of its distribution. Figure 2 shows a typical element of distributed dislocations, located at x_k.

Figure 2

Thus, the corrective terms, $\sigma_{iy,j}^{corr}$ (*i*=*x*,*y*), evaluated at a generic location x_j are:

$$\begin{bmatrix}\sigma_{yy,j}^{corr}\\ \sigma_{xy,j}^{corr}\end{bmatrix} = A_{SM,DM}\sum_{k=1}^{n_p}\int_{\frac{3}{2}x_j-\frac{x_{j+1}}{2}}^{\frac{3}{2}x_{j+1}-\frac{x_j}{2}} B_{x_k}(\xi,x_k)\begin{bmatrix}G_{yy}(x_j,\xi)\\ G_{xy}(x_j,\xi)\end{bmatrix}d\xi. \tag{21}$$

The formulation can be further simplified to obtain:

$$\begin{aligned}\begin{bmatrix}\sigma_{yy,j}^{corr}\\ \sigma_{xy,j}^{corr}\end{bmatrix} &= A_{SM,DM}\sum_{k=1}^{n_p}B_{x_k}\int_{\frac{3}{2}x_j-\frac{x_{j+1}}{2}}^{x_k}\left(1+\frac{x_k}{x_{j+1}-x_j}\right)\begin{bmatrix}G_{yy}(x_j,\xi)\\ G_{xy}(x_j,\xi)\end{bmatrix}d\xi + \\ &+A_{SM,DM}\sum_{k=1}^{n_p}B_{x_k}\int_{x_k}^{\frac{3}{2}x_{j+1}-\frac{x_j}{2}}\left(1-\frac{x_k}{x_{j+1}-x_j}\right)\begin{bmatrix}G_{yy}(x_i,\xi)\\ G_{xy}(x_i,\xi)\end{bmatrix}d\xi,\end{aligned} \tag{22}$$

where the only unknowns are the triangle heights, B_{x_k}, and hence

$$\begin{bmatrix}\sigma_{yy,j}^{corr}\\ \sigma_{xy,j}^{corr}\end{bmatrix} = A_{SM,DM}\sum_{k=1}^{n_p}B_{x_k}\begin{bmatrix}F_{xyjk}\\ F_{yyjk}\end{bmatrix}, \tag{23}$$

with F_{xyjk} and F_{yyjk} given by:

$$\begin{aligned}\begin{bmatrix}F_{xyjk}\\ F_{yyjk}\end{bmatrix} &= \int_{\frac{3}{2}x_j-\frac{x_{j+1}}{2}}^{x_k}\left(1+\frac{x_k}{x_{j+1}-x_j}\right)\begin{bmatrix}G_{yy}(x_j,\xi)\\ G_{xy}(x_j,\xi)\end{bmatrix}d\xi + \\ &+\int_{x_k}^{\frac{3}{2}x_{j+1}-\frac{x_j}{2}}\left(1-\frac{x_k}{x_{j+1}-x_j}\right)\begin{bmatrix}G_{yy}(x_j,\xi)\\ G_{xy}(x_j,\xi)\end{bmatrix}d\xi.\end{aligned} \tag{24}$$

F_{xyjk} and F_{yyjk} represent the influence functions of a dislocation triangle centred at x_k and of unit height, B_{x_k}. These functions can be computed and stored at the outset as they depend only on the density grid, x_k.

The condition for the solution of the problem to be unique (10), can be expressed in its discretised form as follows

$$d_{\sup}\sum_{k=1}^{n_p}B_{x_k} = 0. \tag{25}$$

3.1.2 Quadratic Form of the Minimisation Problem

Now that all elements of the layered elastic problem have been discretised, the problem to be

solved can be written as follows

$$\underset{\min}{\tilde{F}} = -\sum_{j=1}^{n_p} \left[\left(\sigma_{xy,j}^{bil} + \sigma_{xy,j}^{corr} \right) \left(h_j' - h_j'' \right) + f \left(\sigma_{yy,j}^{bil} + \sigma_{yy,j}^{corr} \right) \left(h_j' + h_j'' \right) \right] d_{\text{sup}} \tag{26}$$

where $\sigma_{iy,j}^{corr}$ is given by equation (23) provided only that

$$h_j', h_j'' \geq 0. \tag{27}$$

By appropriately grouping and re-writing the variables of the system under consideration in vector form, x_{quad}, the formulation of the problem to be solved using quadratic programming routines can be expressed as follows:

$$\min_{x_{quad}} \frac{1}{2} x_{quad}^T H_{quad} x_{quad} + f_{quad}^T x_{quad}, \tag{28}$$

where the square matrix H_{quad} includes the quadratic terms of the formulation and the vector f_{quad} the linear terms (these are reported in Appendix B). Likewise, the boundary conditions of our contact problem may be written in matrix form (see Appendix B). This way of writing the problem is useful when commercial routines are applied to find the solution to the problem (e.g. the authors have built their solver using the MATLAB toolbox and its available quadratic programming routines). The reader may refer to Appendix B for a complete description of the numerical approach developed and presented here.

3.2 Moving loads

When the applied loads are stationary in space and either constant or oscillating in time, it is impossible for slip displacement to accumulate to produce a net displacement of the layer with respect to the substrate, but when the applied loads move this is no longer true, and incremental creep, or "ratchetting", can take place. The formulation differs only in equations (8) and (10). In fact, the sign of the relative velocity between layer and substrate, $\dot{h}$, is now the same as the sign of dislocation density, i.e. $sgn(\dot{h}(x)) = sgn(B_x(x))$. This implies that the functional (12) can be written as

$$\tilde{F}_M = \int_{-\infty}^{+\infty} \left\{ - \left[\sigma_{xy}(x,0) B_x(x) + f \sigma_{yy}(x,0) |B_x(x)| \right] \right\} dx \tag{29}$$

This may also be shown to be positive definite, but the functional has to be discretised differently. Similarly, equation (14) may be used as present functional, but with h_j replaced by

B_k

$$\tilde{F}_M = -\sum_{k=1}^{n_p} \left[\left(\sigma^{bil}_{xy,k} + \sigma^{corr}_{xy,k} \right) B_{x_k} + f\left(\sigma^{bil}_{yy,k} + \sigma^{corr}_{yy,k} \right) |B_{xk}| \right] \tag{30}$$

where $\sigma^{corr}_{iy,k} = \sigma^{corr}_{iy,j}/2 + \sigma^{corr}_{iy,j+1}/2$ and $\sigma^{bil}_{iy,k} = \sigma^{bil}_{iy,j}/2 + \sigma^{bil}_{iy,j+1}/2$.

Then, we substitute the discretised form of the dislocation density (20) into (29) to obtain

$$\tilde{F}_M = -\sum_{k,j=1}^{n_p} \left[\left(\sigma^{bil}_{xy,k} + \sigma^{corr}_{xy,k} \right) \frac{h_j - h_{j+1}}{x_{j+1} - x_j} + f\left(\sigma^{bil}_{yy,k} + \sigma^{corr}_{yy,k} \right) \left| \frac{h_j - h_{j+1}}{x_{j+1} - x_j} \right| \right] \tag{31}$$

The difference $h_j - h_{j+1}$ can be replaced by ζ_j and, as $(x_{j+1} - x_j)$ is a positive quantity, it can be removed from the functional, giving

$$\tilde{F}_M = -\sum_{k,j=1}^{n_p} \left[\left(\sigma^{bil}_{xy,k} + \sigma^{corr}_{xy,k} \right) \zeta_j + f\left(\sigma^{bil}_{yy,k} + \sigma^{corr}_{yy,k} \right) |\zeta_j| \right]. \tag{32}$$

This time it is the presence of the absolute value of the relative displacement, ζ_j which complicates the formulation, and it is replaced using the same procedure as that described above, *mutatis mutandis*, so that the problem can be written as follows:

$$\underset{\min}{\tilde{F}_M} = -\sum_{k,j=1}^{n_p} \left[\left(\sigma^{bil}_{xy,k} + \sigma^{corr}_{xy,k} \right) \left(\zeta'_j - \zeta''_j \right) + f\left(\sigma^{bil}_{yy,k} + \sigma^{corr}_{yy,k} \right) \left(\zeta'_j + \zeta''_j \right) \right] \tag{33}$$

where:

$$\begin{aligned} \begin{bmatrix} \sigma^{corr}_{yy,j} \\ \sigma^{corr}_{xy,j} \end{bmatrix} &= A_{SM,DM} \sum_{k,j=1}^{n_p} \frac{\zeta_j}{x_{j+1} - x_j} \int_{\frac{3}{2}x_j - \frac{x_{j+1}}{2}}^{x_k} \left(1 + \frac{x_k}{x_{j+1} - x_j} \right) \begin{bmatrix} G_{yy}(x_j, \xi) \\ G_{xy}(x_j, \xi) \end{bmatrix} d\xi + \\ &+ A_{SM,DM} \sum_{k,i=1}^{n_p} \frac{\zeta_j}{x_{j+1} - x_j} \int_{x_k}^{\frac{3}{2}x_{j+1} - \frac{x_j}{2}} \left(1 - \frac{x_k}{x_{j+1} - x_j} \right) \begin{bmatrix} G_{yy}(x_j, \xi) \\ G_{xy}(x_j, \xi) \end{bmatrix} d\xi \end{aligned} \tag{34}$$

subject to:

$$\sum_{k=1}^{n_p} B_{x_k} (x_{j+1} - x_j) = d \tag{35}$$

$$\zeta'_j, \zeta''_j \geq 0, \tag{36}$$

where d is the net slip accumulated after one passage of the load. Following the same procedure described in the previous section, the problem can be rewritten in a quadratic form and solved using commercial routines.

4 Model validation

4.1 Stationary loads

Extensive comparisons and test cases have been performed, to check the correctness of the formulation and its implementation. These include, for example, the problem of uniform compression, everywhere, applied to the surface of a strip pressed onto an elastically similar half-plane, and with a normal line force, N, applied at the origin at the free surface, Figure 3(a).

Figure 3

The bilateral solution to the elastic contact problem is

$$\sigma_{xy}^{bil}(x) = +\frac{2N}{\pi b}\frac{b^3 x}{\left(b^2+x^2\right)^2} \tag{37}$$

$$\sigma_{yy}^{bil}(x) = -\frac{2N}{\pi b}\frac{b^4}{\left(b^2+x^2\right)^2} - p_0 \tag{38}$$

where b is the layer thickness, N, the normal load applied to the system and p_0 the uniform constant pressure, or, in dimensionless terms

$$\frac{b\sigma_{xy}^{bil}(\tilde{x})}{N} = +\frac{2}{\pi}\frac{\tilde{x}}{\left(1+\tilde{x}^2\right)^2} \tag{39}$$

$$\frac{b\sigma_{yy}^{bil}(\tilde{x})}{N} = -\frac{2}{\pi}\frac{1}{\left(1+\tilde{x}^2\right)^2} - \frac{1}{\lambda_N} \tag{40}$$

where $\tilde{x} = x/b$ and $\lambda_N = N/\left(bp_0\right)$. It is assumed that the surface pressure is applied first and then the line force is increased from zero to a particular value. Figure 4 shows the slip regions predicted with the formulation described, for $f = 0.25$ and $\lambda_N = 2$, compared with the results achieved with the classic iterative scheme based on an integral equation formulation and exploiting the symmetry in x [11]. λ_N is here treated as an unknown of the problem [11]. On the same graph, results for a tensile force, where $\lambda_N = 1.1$ and $f = 0.4$, are plotted [11]. The figure shows the accuracy of the numerical scheme in capturing the location and the extent of the slip region, the local relative displacement and the shear stress distribution at the layer/substrate interface.

Figure 4

A variant on this problem is to apply a monotonically increasing surface shearing force, Q, applied at the origin at the free surface, as depicted in Figure 3(b). This gives a state of interfacial tractions, which can be expressed in dimensionless form as:

$$\frac{b\sigma_{xy}^{bil}(\tilde{x})}{Q} = +\frac{2}{\pi}\frac{\tilde{x}^2}{(1+\tilde{x}^2)^2} \tag{41}$$

$$\frac{b\sigma_{yy}^{bil}(\tilde{x})}{Q} = -\frac{2}{\pi}\frac{\tilde{x}}{(1+\tilde{x}^2)^2} - \frac{1}{\lambda_Q} \tag{42}$$

where now $\lambda_Q = Q/bp_0$. Figure 5 shows the results obtained with our formulation for $\lambda_Q = 2.36$ and $f = 0.5$, plotted together with the results calculated with the classical semi-analytical iterative scheme. Also, in this case, the results are shown to match the semi-analytical results obtained using the formulation in [11].

Figure 5

4.2 Cyclic loading - Tangential load - similar materials

So far, the load has been increased monotonically. In the following example case, whose geometry and loading conditions are schematically described in the insets to Figure 6, the tangential load is initially set to reproduce the monotonic loading scenario shown in Figure 3(b) and whose results are reported in Figure 5 for $\lambda_Q = 2.36$ and $f = 0.5$. The load is then first fully reversed ($\lambda_Q = -2.36$, point 2 of the loading cycle in the inset to Figure 6) and cycled ($\lambda_Q = -2.36 \leftrightarrows 2.36$, point 3 of the loading cycle in the inset to Figure 6). This example enables us to show how the methodology developed allows tracking the "marching-in-time" solution without having to guess the evolution of the extent and the location of the slip regions which would require rather cumbersome iterative routines. The loading scenario used as a vehicle for our investigation was first explored by Comninou and Barber [9], who, based on the numerical results obtained during their investigation, first introduced the frictional shakedown concept - and its analogy with plastic shakedown - in the context of layered frictional systems.

The tractions at the interface when the load is monotonically increased are given by the solution of the monotonic loading case and they are here referred to with the index 1 (as they refer to point 1 of the loading cycle in the inset to Figure 6). When the tangential load is

reduced, the solution to the problem (point 2 in Figure 6) can be written in dimensionless form, as follows[2]:

$$\begin{bmatrix} \dfrac{b\sigma^2_{yy}(\tilde{x},0)}{Q_1} \\ \dfrac{b\sigma^2_{xy}(\tilde{x},0)}{Q_1} \end{bmatrix} = \begin{bmatrix} \dfrac{b\sigma^1_{yy}(\tilde{x},0)}{Q_1} \\ \dfrac{b\sigma^1_{xy}(\tilde{x},0)}{Q_1} \end{bmatrix} + \begin{bmatrix} \dfrac{2}{\pi}\Delta Q \dfrac{\tilde{x}^2}{\left(1+\tilde{x}^2\right)^2} \\ -\dfrac{2}{\pi}\Delta Q \dfrac{\tilde{x}}{\left(1+\tilde{x}^2\right)^2} \end{bmatrix} + \begin{bmatrix} \sigma^{corr,2}_{yy}(\tilde{x}) \\ \sigma^{corr,2}_{xy}(\tilde{x}) \end{bmatrix}, \tag{43}$$

where ΔQ is the difference between Q_1 and Q^*, with Q^* being $2Q_1$ (see Figure 6), $\sigma^1_{yy}(\tilde{x},0)$ and $\sigma^1_{xy}(\tilde{x},0)$ are the corrected stress field for the condition 1, and $\sigma^{corr,2}_{yy}(\tilde{x})$ and $\sigma^{corr,2}_{xy}(\tilde{x})$ the corrective terms to be superposed to modify the Flamant solution [32] introduced for condition 2. The solutions for the following time steps (starting from point 3 in Figure 6) can be calculated using exactly the same procedure.

Figure 6 shows the results for both the unloading part of the tangential loading cycle (point 2 in Figure 6) and for the first re-loading trajectory (point 3 in Figure 6) computed by the means of our numerical scheme for $\lambda_Q = 2.36$. The outputs are plotted in terms of normalised shear tractions at the interface between the layer and the substrate along with the results achieved with the classical iterative scheme employed by Comninou and Barber [9]. The colour code (red for point 2 and black for point 3) is preserved in the curves and the data points displayed in the graph with the aim to aid the interpretation of the results. The match between the results obtained with the quadratic programming technique and the classical formulation is very satisfactory.

Figure 6

As already mentioned, results reported in [9] were calculated for values of pressure such that the frictional law was violated along the layer/substrate interface at only limited positions throughout the cycle. Subsequently, further investigations were limited to simplified loading scenarios. This limitation is here circumvented by the use of the quadratic programming formulation permitting many other loading regimes to be investigated. Figure 7 shows an example case where multiple slip areas are simultaneously present during the loading and the unloading

[2] Note that the solution at the extremes of the loading cycle is always used as the starting point for the subsequent monotonically increasing or decreasing loading trajectories. Starting from the previously established state implies that the corrective problem being solved at any given stage does satisfy equation (3) and that the locked-in residual stresses are adequately captured by the solution.

phases. In this case, the values of the tangential force, Q, have been set to oscillate such that λ_Q varies between $\pm\, 3.2$. As a result of the increase in the maximum applied load, the contact between the layer and the substrate is initially characterised by an area where relative (forward) slip displacements take place which is larger with respect to the slip region shown in Figure 5 (point 1 of the loading cycle in the inset to Figure 7). This area is delimited by the shaded blue rectangle in Figure 7. Upon unloading and subsequent re-loading (point 2 and 3 of the loading cycle depicted in the inset to Figure 7), two areas where slip occurs nucleate and evolve at either side of the point of application of the load. Note again that the color code indicates the point of the cycle to which the solutions and the areas of slip correspond to (blue for point 1, red for point 2 and black for point 3). The solution evolves between having slip areas characterised alternatively by backward and forward slip until a steady-state is reached; this corresponds to point 3 in Figure 7. At this stage the system has shakendown and subsequent unloading and re-loading will show the same slip areas and traction distributions obtained at point 3. It should be noted that the slip areas and the shear tractions will be obviously mirrored horizontally and both slip directions and tractions will change sign and give rise to backward slip and negative tractions at the end of the subsequent unloading phases.

Figure 7

The numerical scheme proposed has also been applied to the more practical class of contact problems already investigated by the authors [15]. A schematic of the contact problem is shown in the inset to Figure 8. The two-dimensional contact model consists of an elastic strip, resting on a substrate, and subjected to different rolling contact conditions caused by contact between the layer and a disc [15]. The interfacial friction coefficient between strip and substrate, f, differ from the friction coefficient between disk and layer, μ. An example case is shown in Figure 8 where $f = 0.2$, $\mu = 0.7$ and $\lambda = 1$, where λ is a function of the constant pressure[3], p_0, uniformly applied to the layer surface. In this case the layer is elastic whilst the substrate is rigid. As can be seen from the figure, the match between the results is very satisfactory for this

[3] $\lambda = p_0/p_H$. H stands for Hertzian and it should be noted here that the Hertzian case has been chosen as a reference for the normalised variables. It corresponds to the case when the strip thickness $b \to \infty$. p_H and the Hertzian contact area, a_H, are, therefore, easily computed once the geometry, the applied normal load and elastic properties of the strip are known [15].

case.

Figure 8

4.3 Moving loads

An extension of the technique described above from stationary loads to model moving loads [13] was developed. The numerical scheme had been first validated against the case shown in Figure 3, where the compressive normal load is now moved along the layer surface at constant speed. The case was treated in [13], where it is shown that, in general, two slip zones are always present at the interface between layer and substrate. The displacements accumulated in the two slip zones are opposite in sign, and Figure 9 shows an example case where the results obtained for $\lambda_N = 8$ and $f = 0.5$ are plotted, together with the results calculated using the classical semi-analytical iterative scheme based on the integral equation approach [13]. It should be noted that the classical semi-analytical scheme requires initial guesses for the location and size of each individual slip zone and proceeds by iteration, and "this is practically impossible unless there are some clues" [13]. This problem is overcome here as both size and location of the slip zones are automatically detected using the proposed quadratic programming formulation.

Figure 10 shows a dimensionless measure of the net displacement, d, accumulated between layer and substrate as a function of the dimensionless contact pressure, λ_N, for $f = 0.5$[4]. The match between the results is again very satisfactory.

Figure 9

Figure 10

The numerical scheme has also been validated against the equivalent results for the contact problem illustrated in the inset to Figure 8 where the disc is now moved along the surface of the layer. Figure 11 shows the results obtained using the present formulation and the marching-in-time solution developed in [15] for a normalised net displacement $Cd/(p_H a_H) = 0.184$, $\mu = 0.7$, $f = 0.2$ and $\lambda = 1$. The comparison between the two sets of results shows again the

[4] Note that the accumulated net displacement, d, corresponds to corresponds to the sum of the contributions from the two slip areas ($d = d_1 + d_2$ from Fig. 9). This corresponds to a negative net displacement (opposite with respect to the rolling direction - hence the negative sign) for the conditions shown in Fig. 10.

accuracy of the proposed numerical scheme.

Figure 11

5 Experimental investigation of creep and model corroboration

This novel numerical tool has proved to be accurate and capable of resolving different loading scenarios. It has also been shown to be superior to standard iterative approaches, especially when multiple slip areas are generated in the presence of moving loads. These problems are not easily tackled by techniques which rely on conventional integration schemes [15]. In order to test our numerical approach further, an experimental investigation was carried out. Tests were performed by modifying an apparatus conventionally adopted to study micropitting [33]. The rig is shown in Figure 12 and has two main rotating shafts. The first shaft carries a large disk which drives three smaller shafts, whilst the second shaft drives the central disc against which the three rollers driven by the first shaft are pressed. Torque-meters are mounted on the two main shafts in order to monitor and regulate the torque applied to the rollers.

Experimental results were obtained by testing tyred rollers in geometrical and loading configurations which give rise to incremental slip of the tyre around the roller. The experimental configuration described above is capable of reproducing loading conditions similar to those simulated in [13] and [15], as illustrated in Figures 8-11. The three rollers mounted on the first shaft are made of mild steel ($178HV$) and have shrink fitted steel tyres. The tyred rollers are denoted top ring, left ring and right ring (ring internal radius $26.30mm$; thickness $0.08mm$; width $5mm$; and average interference $30-50\mu m$). The resulting test configuration recalls the cases investigated in [16], [28] and [29], where an elastic layer was pressed onto an elastically similar substrate. In the inset to Figure 12, the schematic of the contact problem under investigation is illustrated. This can be directly linked to those shown in Figure 3(a) and in the inset to Figure 11 under the Hertzian and half-plane assumptions [15] [16]. The components are accurately manufactured so to guarantee a well controlled interference fit between roller and tyres (with roughness characterised by $R_{a,disk} = 0.82\ \mu m$; $R_{a,ring} = 1.31\ \mu m$). The tests were run under pure rolling condition [13] [28]. Frictional properties of the layer-substrate interface have been investigated and the interfacial friction coefficient was measured by monitoring the

compressive force required to press the rings onto the discs. The press-fit was carried out using a standard INSTRON test apparatus - *www.instron.co.uk*. During the fitting process, the relative displacement between disk and ring was carefully recorded, together with the pressing force. The friction coefficient was then estimated by dividing the resultant radial force found from interference calculations by the measured load used to press-fit the tyred disks[5]. The final value corresponds to the elastic layer fully mounted on the roller and is, therefore, the coefficient of friction that characterises the coupling. This is the value used subsequently to simulate the system using analytical or numerical approaches. It should be also noted here that, in order to reduce the friction coefficient between roller and tyres, a layer of dry spray coating (Molycote D321 - *www.dowcorning.com*) was applied at the contact interface between the steel rings and the steel rollers. This reduced the friction coefficient so that creep occurred at lower values within the load range of the MPR test apparatus. Other surfaces were tested as received. The net displacement between the rollers and the tyres was obtained by tracking the relative mis-alignment between two surfaces marks which were applied across the interface between the two elements after the mounting process. The displacement of the tyres with respect to the rollers was found to increase in direct proportion to the number of revolutions.

Figure 12

Figure 13 shows a series of experimental results where dimensionless value of the incremental creepage, characterised by the dimensionless value of the net displacement per revolution, d, obtained for different values of the layer/substrate friction coefficient, f, is plotted against, λ_N, i.e. as a function of the constant pressure uniformly applied to the layer, p_0. The quantities d and p_0 are normalized with respect to the normal load applied to the counter-disc, N (*load=120N/mm*), the shear modulus of the material, G, the Kolosov's constant, κ, and the layer thickness, b *(0.08mm)*. Also reported in Figure 13 are the predictions obtained using the numerical technique developed in this paper. The agreement between the model and the experiments demonstrates that the model is able to capture the behavior of the system. The minor

[5] Note that values of the load used to calculate the friction coefficient were those recorded towards the end of the fitting process, *i.e.* when the instabilities linked to the mounting process had been overcome and the effect of the singularities at the corners became negligible.

discrepancies in the results are mainly due to the uncertainties in measurement of the coefficient of friction between layer and substrate. Experimental results obtained by Anscombe and Johnson in 1974 for the same kinematic con guration, pure rolling, are plotted in the inset to Figure 13 [28]. As already discussed in [13], the experiments show net displacements which are not perfectly in line with the model predictions assuming that the range of friction coefficients measured are in the $0.1 - 0.15$ range [13]. The discrepancy between the numerical results and the experimental data can be attributed to misalignment, variations in the average friction coef cients measured during the press-fitting process and the (lower) coefficients which could be more appropriate to describe the interfacial slip due to the moving force, and to the presence of plasticity when large normal forces are applied (see blue diamonds and red squares in Figure 13).

Figure 13

6 Conclusions

An effective numerical method based on the distributed dislocation technique and on a quadratic programming formulation has been developed to investigate interfacial slip in layered systems. The numerical scheme has been successfully tested against classical problems and has been shown to be accurate and efficient. It overcomes the drawbacks of standard semi-analytical iterative schemes, thus enabling us to extend the applicability of the distributed dislocation technique to the solution of complex two-dimensional layered systems when slip is present at the mating interfaces. The proposed approach has been shown to be able to capture the initiation and the evolution of multiple slip regions at the layer/substrate interface in the presence of moving loads and has been also applied to study rolling contact of tyred systems. We have shown that, in such systems, the proposed methodology can be used to model accurately interfacial creep by performing quantitative comparisons between our numerical outputs and the experimental results obtained using an in-house test rig.

7 Acknowledgments

The support of the UK Technology Strategy Board (grant TP/5/MAT/6/I/H0324L) is gratefully acknowledged by SR and DD.

8 Appendix A

The influence functions associated with a single glide dislocation located at the interface between two similar/dissimilar materials are given.

When the materials are similar, with similar meaning having the same Poisson's ratio and the same Young's modulus, the expressions for the influence functions and the constant A to be substituted into (22) are

$$G_{yy}(x,\xi) = 16\left(-\frac{3b^3}{\left[4b^2+(x-\xi)^2\right]^2}+\frac{16b^5}{\left[4b^2+(x-\xi)^2\right]^2}\right) \tag{44}$$

$$G_{xy}(x,\xi) = 2\left(\begin{array}{c}\dfrac{1}{x-\xi}-\dfrac{x-\xi}{4b^2+(x-\xi)^2}+\\ +\dfrac{12b^2(x-\xi)}{\left[4b^2+(x-\xi)^2\right]^2}-\dfrac{64b^4(x-\xi)}{\left[4b^2+(x-\xi)^2\right]^3}\end{array}\right) \tag{45}$$

$$A_{SM} = \frac{2E}{\pi(\kappa+1)} \tag{46}$$

where

$$\kappa = 3-4\nu \tag{47}$$

When the materials are dissimilar, if the layer is indicated with 1 and substrate with 2, the influence functions and the material constant A can be expressed as follows

$$G_{xy}(x,\xi) = \frac{1}{x-\xi}-\frac{1-\alpha}{2b}\int_0^\infty \frac{N_{12}}{D_{22}}e^{-\tau}\sin\left(\frac{x-\xi}{BA}\tau\right)d\tau \tag{48}$$

$$G_{yy}(x,\xi) = -\pi\beta\delta(x-\xi)+\frac{1-\alpha}{2b}\int_0^\infty \frac{N_{22}}{D_{22}}e^{-\tau}\sin\left(\frac{x-\xi}{BA}\tau\right)d\tau \tag{49}$$

$$A_{DM} = \frac{2E_2(1-\alpha)}{(\kappa_2+1)\left(1-\beta^2\right)} \tag{50}$$

where

$$N_{12} = 4\left[\left(1+\beta^2\right)\tau^2+\beta\right]e^{\tau}-2\beta(1+\alpha)e^{-\tau} \tag{51}$$

$$N_{22} = 2\left\{2(1+\beta)\left[(1+\beta)\tau-(1-\beta)\right]\tau+1+\beta^2\right\}e^{\tau}-2\left(\alpha+\beta^2\right)e^{-\tau} \tag{52}$$

$$D_{12} = D_{22} = \left(1-\beta^2\right)e^{2\tau} + \left(\alpha^2-\beta^2\right)e^{-2\tau} - 4\left(1+\beta\right)\left(\alpha-\beta\right)\tau^2 - 2\left(\alpha-\beta^2\right) \tag{53}$$

$$\kappa_2 = 3 - 4\nu_2 \tag{54}$$

α and β are the Dundur's parameters, which can be expressed as follows

$$\alpha = \frac{E_2\left(\kappa_1+1\right) - E_1\left(\kappa_2+1\right)}{E_2\left(\kappa_1+1\right) + E_1\left(\kappa_2+1\right)} \tag{55}$$

$$\beta = \frac{E_2\left(\kappa_1-1\right) - E_1\left(\kappa_2+1\right)}{E_2\left(\kappa_1+1\right) + E_1\left(\kappa_2+1\right)} \tag{56}$$

The advantage of expressing the materials parameters of a generic bimaterial composite undergoing plane deformation, speci cally Young's modulus and Poisson's ratio, into two parameters, α and β, is that the stress field can be shown to be dependent on these two parameters only [14].

9 Appendix B

In this appendix we illustrate how the solution to contact problem subjected to linear equalities and linear inequalities as formulated by the authors, i.e. expressed in terms of a quadratic function to be minimised, may be found using MATLAB and/or similar commercial software which allow implementing quadratic programming routines. The formulation for the steady stationary case is illustrated here and the numerical routine for the moving load case may be obtained analogously.

The quadratic programming algorithm implemented in MATLAB allows finding a solution for the following class of mathematical problems:

$$\min_{x_{quad}} \frac{1}{2} x_{quad}^T H_{quad} x_{quad} + f_{quad}^T x_{quad} \tag{57}$$

such that

$$A_{Lie} x_{quad} \leq b_{Lie} \tag{58}$$

$$l_b \leq x_{quad} \leq x_b \tag{59}$$

$$A_{Le}x_{quad} = b_{Le} \tag{60}$$

where H_{quad} is the matrix and f_{quad} the vector that contain respectively the quadratic and the linear terms of the functional to be minimised, and the variables of the problem are grouped into vector x_{quad}. The boundary conditions required to guarantee the uniqueness of the solution are expressed in terms of linear inequalities, (58) and/or (59), and linear equalities, (60). A_{Lie} (*Lie: linear inequality*) and A_{Le} (*Lie: linear equality*) are matrices while b_{Lie} b_{Le} l_b x_b are vectors.

As already mentioned in section 3.1.2 (see (28)), the first step to solve the problem under consideration is to re-write the functional form (26) in the matrix form equivalent to (57). Hence, if we divide the functional (26) into its quadratic, $\tilde{F}_{quadratic}$, and its linear part, $\tilde{F}_{linear}$, as follows:

$$\tilde{F}_{quadratic} = -\sum_{j=1}^{n_p} \left[\sigma_{xy,j}^{corr}\left(h'_j - h''_j\right) + f\sigma_{yy,j}^{corr}\left(h'_j + h''_j\right)\right] d_{\sup} \tag{61}$$

$$\tilde{F}_{linear} = -\sum_{j=1}^{n_p} \left[\sigma_{xy,j}^{bil}\left(h'_j - h''_j\right) + f\sigma_{yy,j}^{bil}\left(h'_j + h''_j\right)\right] d_{\sup}, \tag{62}$$

The vectors x_{quad}^T, f_{quad}^T and the matrix H_{quad} (see (28)) may then be defined as:

$$x_{quad}^T = \left[h'_1 \dots h'_{n_p}, h''_1 \dots h''_{n_p}, \sigma_{xy,1}^{corr} \dots \sigma_{xy,n_p}^{corr}, \sigma_{yy,1}^{corr} \dots \sigma_{yy,n_p}^{corr}, B_{x_1} \dots B_{x_{n_p}}\right], \tag{63}$$

$$f_{quad}^T = \left[-\sigma_{xy,1}^{bil} - f\sigma_{yy,1}^{bil} \dots -\sigma_{xy,n_p}^{bil} - f\sigma_{yy,n_p}^{bil}, \sigma_{xy,1}^{bil} - f\sigma_{yy,1}^{bil} \dots \sigma_{xy,n_p}^{bil} - f\sigma_{yy,n_p}^{bil}, 0 \dots 0, 0 \dots 0, 0 \dots 0\right], \tag{64}$$

$$H_{quad} = \begin{bmatrix} [0]_{n_p,n_p} & [0]_{n_p,n_p} & -[I]_{n_p,n_p} & -f\,[I]_{n_p,n_p} & [0]_{n_p,n_p} \\ [0]_{n_p,n_p} & [0]_{n_p,n_p} & [I]_{n_p,n_p} & -f\,[I]_{n_p,n_p} & [0]_{n_p,n_p} \\ -[I]_{n_p,n_p} & [I]_{n_p,n_p} & [0]_{n_p,n_p} & [0]_{n_p,n_p} & [0]_{n_p,n_p} \\ -f\,[I]_{n_p,n_p} & -f\,[I]_{n_p,n_p} & [0]_{n_p,n_p} & [0]_{n_p,n_p} & [0]_{n_p,n_p} \\ [0]_{n_p,n_p} & [0]_{n_p,n_p} & [0]_{n_p,n_p} & [0]_{n_p,n_p} & [0]_{n_p,n_p} \end{bmatrix}, \tag{65}$$

where $[0]_{n_p,n_p}$ and $[I]_{n_p}$ represent the zero $n_p \times n_p$ matrix and the identity matrixes of order $n_p \times n_p$ respectively[6].

[6] It should be noted here that the number of variables in x_{quad} could have been reduced by

Now, we turn our attention to the side conditions which need to be satisfied to find the solution of the problem under investigation. The equalities (23), (20) and (25), and the inequalities which provide the bounds for traction and interfacial displacements, i.e.:

$$|\sigma_{xy}(x,0)| \leq -f\sigma_{yy}(x,0)\,, \tag{66}$$

$$h'_j, h''_j \geq 0, \tag{67}$$

need to be re-written in a matrix form equivalent to (60), (58) and (59).

Let us start from the two linear inequalities (66) and (67) . They can be written in the prescribed matrix form by defining the following vectors and matrixes:

$$l_b^T = [0\ldots0, 0\ldots0, -\infty\ldots-\infty, -\infty\ldots-\infty, -\infty\ldots-\infty]\,, \tag{68}$$

$$x_b^T = [+\infty\ldots+\infty, +\infty\ldots+\infty, +\infty\ldots+\infty, +\infty\ldots+\infty, +\infty\ldots+\infty]\,, \tag{69}$$

$$A_{Lie} = \begin{bmatrix} [0]_{n_p,n_p} & [0]_{n_p,n_p} & [I]_{n_p} & -f\ [I]_{n_p} & [0]_{n_p,n_p} \\ [0]_{n_p,n_p} & [0]_{n_p,n_p} & -[I]_{n_p} & -f\ [I]_{n_p} & [0]_{n_p,n_p} \end{bmatrix}, \tag{70}$$

and

$$b_{Lie}^T = \left[-f\sigma_{yy,1}^{bil} - \sigma_{xy,1}^{bil} \ldots - f\sigma_{yy,n_p}^{bil} - \sigma_{xy,n_p}^{bil}, -f\sigma_{yy,1}^{bil} + \sigma_{xy,1}^{bil} \ldots - f\sigma_{yy,n_p}^{bil} + \sigma_{xy,n_p}^{bil}\right]. \tag{71}$$

Reverting to the linear equalities, (23), (20) and (25) can be written in a matrix form equivalent

incorporating equalities (23) and (20) into (26), therefore limiting the number of unknowns to the displacements h'_j and h''_j. These are indeed the two sets of independent complementarity variables to be determined at every time step. However, re-casting the problem would have rendered the formulation more cumbersome and difficult to follow.

to (60) by setting:

$$A_{Le} = \begin{bmatrix} [0]_{n_p,n_p} & [0]_{n_p,n_p} & [I]_{n_p} & [0]_{n_p,n_p} & A_{SM,DM} \begin{bmatrix} -F_{xy11} & \dots & -F_{xy1n_p} \\ \vdots & \ddots & \vdots \\ -F_{xyn_p1} & \dots & -F_{xyn_pn_p} \end{bmatrix} \\ [0]_{n_p,n_p} & [0]_{n_p,n_p} & [0]_{n_p,n_p} & [I]_{n_p} & A_{SM,DM} \begin{bmatrix} -F_{yy11} & \dots & -F_{yy1n_p} \\ \vdots & \ddots & \vdots \\ -F_{yyn_p1} & \dots & -F_{yyn_pn_p} \end{bmatrix} \\ -[M_1]_{n_p,n_p} & [M_1]_{n_p,n_p} & [0]_{n_p,n_p} & [0]_{n_p,n_p} & d_{\sup}\,[I]_{n_p} \\ 0 & 0 & 0 & 0 & \begin{bmatrix} 1 & \dots & 1 \end{bmatrix} \end{bmatrix}, \tag{72}$$

and

$$b_{Le}^T = [0 \dots 0, 0 \dots 0, 0 \dots 0, 0 \dots 0, 0 \dots 0], \tag{73}$$

with

$$[M_1]_{n_p,n_p} = \begin{bmatrix} 1 & -1 & 0 & \dots & 0 \\ 0 & 1 & -1 & \ddots & \vdots \\ \vdots & 0 & \ddots & \ddots & \vdots \\ \vdots & \ddots & \ddots & \ddots & -1 \\ 0 & \dots & \dots & 0 & 1 \end{bmatrix}. \tag{74}$$

The numerical solver built following the scheme described above is robust and it provides the correct solution to the problem under investigation as long as the physical domain analysed contains all the slip regions developed upon application of the alternating load. Furthermore, setting B_{x_1} or $B_{x_{n_p}}$ to zero in (20), therefore imposing stick at one of the edges of the domain under investigation, may improve numerical stability.

References

[1] Hills, D.A., Nowell, D., and A. Sackfield, *Mechanics of elastic contacts*, Butterworth Heinemann, 1993.

[2] Zografos, A., D. Dini, A. V. Olver, "Fretting fatigue and wear in bolted connections: A multi-level formulation for the computation of local contact stresses", *Tribology International*, 2009, **42**, 1663.

[3] K. Elleuch, H. Proudhon, C. Meunier, S. Fouvry, "Development of a contact compliance method to detect the crack propagation under fretting", *Tribology International*, 2006, **39**, p. 1262.

[4] Barber, J.R., A. Klarbring, and M. Ciavarella, "Shakedown in frictional contact problems for the continuum", *Comptes Rendus Mécanique*, 2008, **336**, p. 34.

[5] Truman, C.E., and J.D. Booker, "Analysis of a shrink-fit failure on a gear hub/shaft assembly", *Engineering Failure Analysis*, 2007, **14**, p. 557.

[6] Antoni, N., Q.S. Nguyen, J.L. Ligier, P. Saffré, and J. Pastor, "On the cumulative microslip phenomenon", *European Journal of Mechanics - A/Solids*, 2007, **26**, p. 626.

[7] Ahn, Y.J., and J.R. Barber, "Response of frictional receding contact problems to cyclic loading", *International Journal of Mechanical Sciences*, 2008, **50**, p. 1519.

[8] Reina, S., D. Dini, and D.A. Hills, "On the accurate prediction of interfacial micro-slip in frictional joints using distributed dislocations and quadratic programming techniques", *Procedia Engineering*, 2009, **1**, p. 181.

[9] Comninou, M., and J.R. Barber, "Frictional slip between a layer and a substrate due to a periodic tangential surface force", *International Journal of Solids and Structures*, 1983, **19**, p. 533.

[10] Comninou, M., J.R. Barber, and J. Dundurs, "Interface slip caused by a surface load moving at constant speed", *International Journal of Mechanical Sciences*, 1983, **25**, p. 41.

[11] Comninou, M., D. Schmueser, and J. Dundurs, "Frictional slip between a layer and a substrate caused by a normal load", *International Journal of Engineering Science*, 1980, **18**, p. 131.

[12] Comninou, M., and J. Dundurs, "Partial closure of cracks at the interface between a layer and a half space", *Engineering Fracture Mechanics*, 1983, **18**, p. 315.

[13] Chang, F.K., M. Comninou, and J.R. Barber, "Slip between a layer and a substrate caused by a normal force moving steadily over the surface", *International Journal of Mechanical Sciences*, 1983, **25**, p. 803.

[14] Dundurs, J., "Effect of Elastic Constants on Stress In A Composite Under Plane Deformation", *Journal of Composite Materials*, 1967, **1**, p. 310.

[15] Reina, S., D. Dini, and D.A. Hills, "Interfacial Slip and Creep in Rolling Contact incorporating a Cylinder with an Elastic Layer", *European Journal of Mechanics - A/Solids*, 2010, In Press, doi:10.1016/j.euromechsol.2010.02.009.

[16] Reina, S., D. Dini, and D.A. Hills, "Incipient slip conditions in rolling contact of tyred wheels", *Proceedings of the IMechE Part C, Journal of Mechanical Engineering Science*, 2010, In Press, doi: 10.1243/09544062JMES2075.

[17]Kalker, J.J., "A minimum principle for the law of dry friction with application to elastic cylinders in rolling contact. Part 1: fundamentals, application to steady state rolling", *Transaction ASME*, *Journal of Applied Mechanics*, 1971, **38**, p. 875.

[18]Kalker, J.J., *Three dimensional elastic bodies in rolling contact*, Kluwer, Dordrecht, 1990.

[19]Klarbring, A., "A mathematical programming approach to three-dimensional contact problems with friction", *Computer Methods in Applied Mechanics and Engineering*, 1986, **58**, p. 175.

[20]Klarbring, A., and G. Björkman, "A mathematical programming approach to contact problems with friction and varying contact surface", *Computers & Structures*, 1988, **30**, p. 1185.

[21]Nowell, D., and D.N. Dai, "Analysis of Surface Tractions in Complex Fretting Fatigue Cycles Using Quadratic Programming", *Journal of Tribology*, 1998, **120**, p. 744.

[22]Maier, G., "A quadratic programming approach for certain classes of non linear structural problems", *Meccanica*, 1968, **3**, p. 121.

[23]Maier, G., "Quadratic programming and theory of elastic-perfectly plastic structures", *Meccanica*, 1968, **3**, p. 265.

[24]Maier, G., "A method for approximate solutions of stationary creep problems", *Meccanica*, 1969, **4**, p. 36.

[25]de Matos, P. F. P., and D. Nowell, "On the accurate assessment of crack opening and closing stresses in plasticity-induced fatigue crack closure problems", *Engineering Fracture Mechanics*, 2007, **74**, p. 1579.

[26]Su, R.K.L., Y. Zhu, and A.Y.T. Leung, "Parametric quadratic programming method for elastic contact fracture analysis", *International Journal of Fracture*, 2002, **117**, p. 143.

[27]Chand, R., "Analysis of unbonded contact problems by means of quadratic programming", *Journal of Optimization Theory and Applications*, 1976, **20**, p. 171.

[28]Anscombe, H., and K.L. Johnson, "Slip of a thin solid tyre press-fitted on a wheel", *International Journal of Mechanical Sciences*, 1974, **16**, p. 329.

[29]Bentall, R.H., and K.L. Johnson, "An elastic strip in plane rolling contact", *International Journal of Mechanical Sciences*, 1968, **10**, p. 637.

[30]Ahn, Y.J., E. Bertocchi, and J.R. Barber, "Shakedown of coupled two-dimensional discrete frictional systems", *Journal of the Mechanics and Physics of Solids*, 2008, **56**, p. 3433.

[31]Qiu, H., D. Dini, and D.A. Hills, "Torsional contact of an elastic flat-ended cylinder", *Journal of the Mechanics and Physics of Solids*, 2008, **56**, p. 3352.

[32]Timoshenko, S. and Goodier, J.N., *Theory of elasticity*, McGraw-Hill, New York, 1970.

[33]E. Lainé, A. V. Olver, T. A. Beveridge, "Effect of lubricants on micropitting and wear", *Tribology International*, 2008, **41**, 1049.

10 Captions to Figures

Figure 1. Schematic of the layered contact problem and possible interface regimes.

Figure 2. Schematic of the layered system and piecewise linear representation of the dislocation density.

Figure 3.Geometry of the present problem and loading conditions: application of a monotonically increasing (a) normal and (b) tangential concentrated load.

Figure 4. Shear tractions and relative displacement between layer and substrate for f=0.25, $\lambda_N = 2$ ($N < 0$) and f=0.4, $\lambda_N = 1.1$ ($N < 0$) - stationary case.

Figure 5. Shear tractions and relative displacement between layer and substrate for f=0.5, $\lambda_Q = 2.36$ - stationary case.

Figure 6. Shear tractions for f=0.5 and $\lambda_Q = \pm 2.36$ (cyclic tangential load) - stationary case.

Figure 7. Shear tractions for f=0.5 and $\lambda_Q = \pm 3.2$ (cyclic tangential load) - stationary case.

Figure 8. Shear tractions and relative displacement between layer and substrate for B=1, f=0.2, $\mu = 0.7$, $\lambda = 1$ and $\nu = 0.3$ - stationary case - full sliding of a roller over the layer surface.

Figure 9. Shear tractions and relative net displacement between layer and substrate for λ_N=8, for f=0.5.

Figure 10. Relative net displacement between layer and substrate as a function of the dimensionless constant pressure, λ_N, for f=0.5.

Figure 11. Shear tractions and relative net displacement between layer and substrate for B=1, f=0.2, $\mu = 0.7$, $\lambda = 1$ and $\nu = 0.3$ - steady state solution for the moving load case - full sliding of a roller over the layer surface.

Figure 12. PCS MPR (*www.pcs-instruments.com/mpr*) experimental apparatus consisting of three tyred rollers and a central roller and schematic of the loading system.

Figure 13. Net displacement, d, per revolution as a function of the dimensionless constant pressure, λ, and of the interfacial friction coef cient, f. In the same graph, comparison with experimental results and, in the inset, with Anscombe's original data (Anscombe and Johnson, 1974; and Chang et al., 1983).

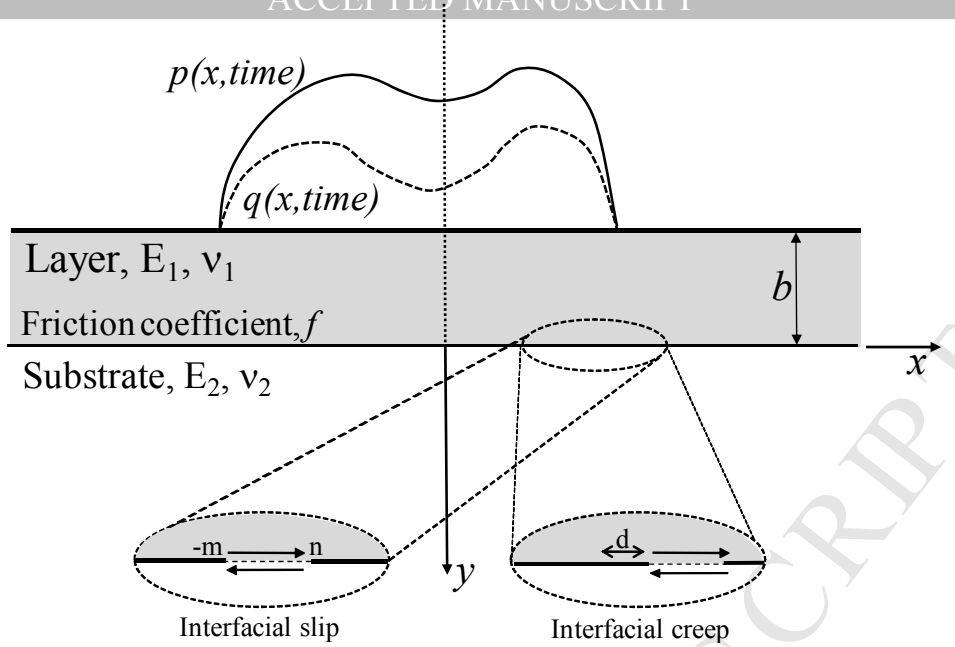

Figure 1. Schematic of the layered contact problem and possible interface regimes.

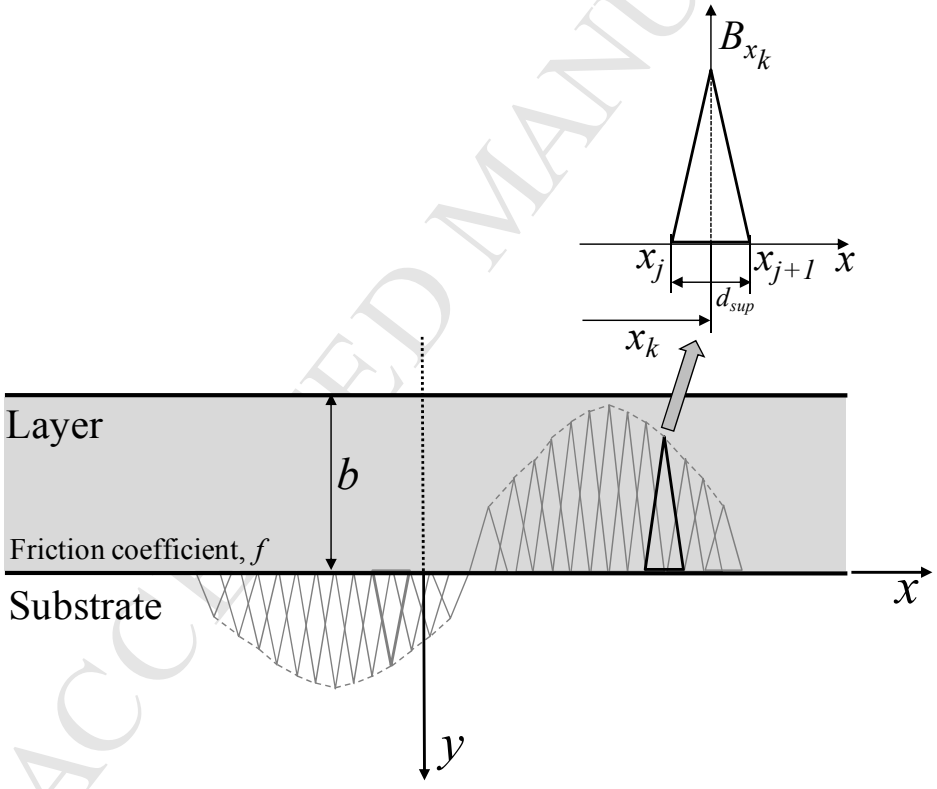

Figure 2. Schematic of the layered system and piecewise linear representation of the dislocation density.

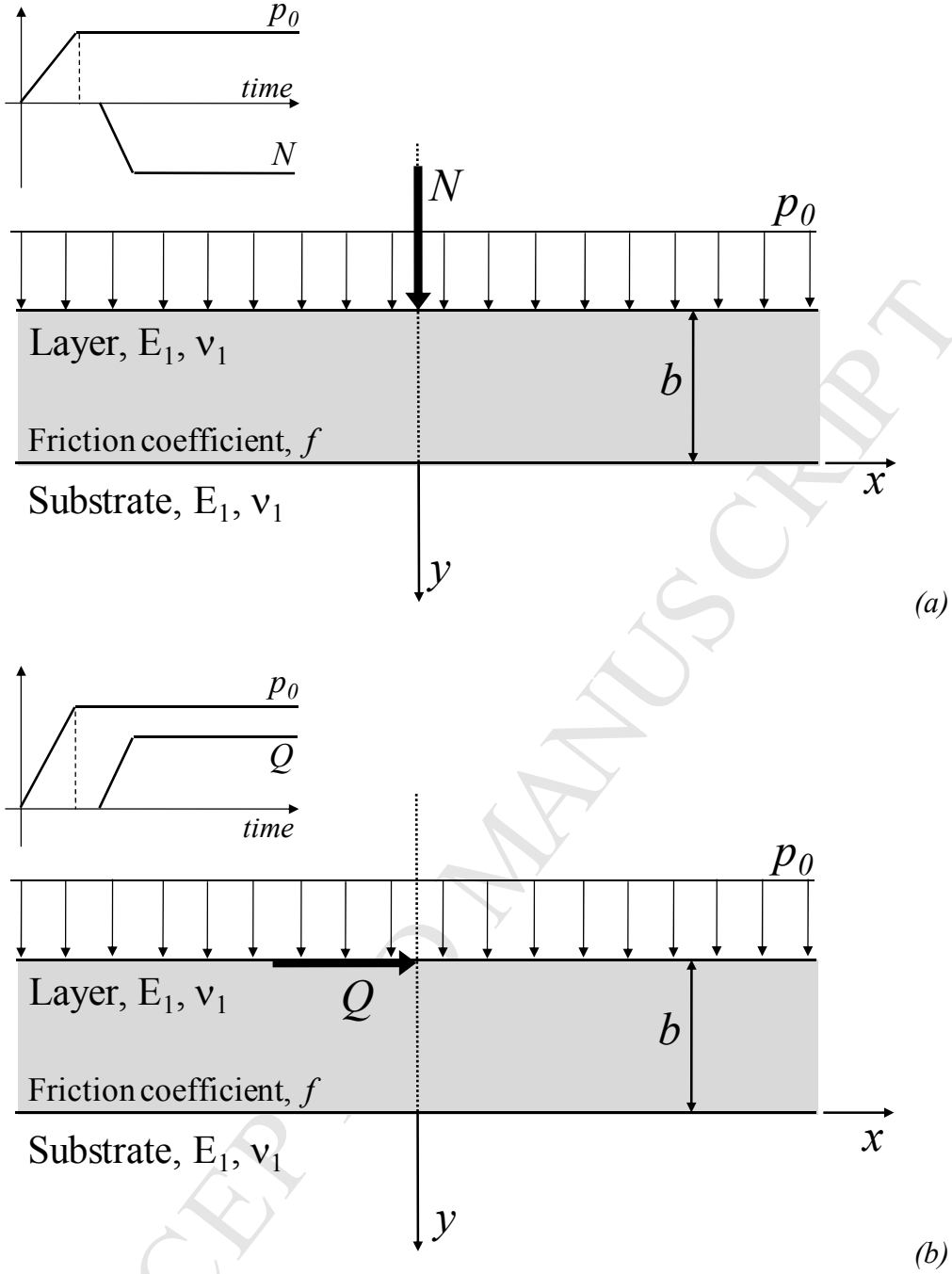

Figure 3.Geometry of the present problem and loading conditions: application of a monotonically increasing (a) normal and (b) tangential concentrated load.

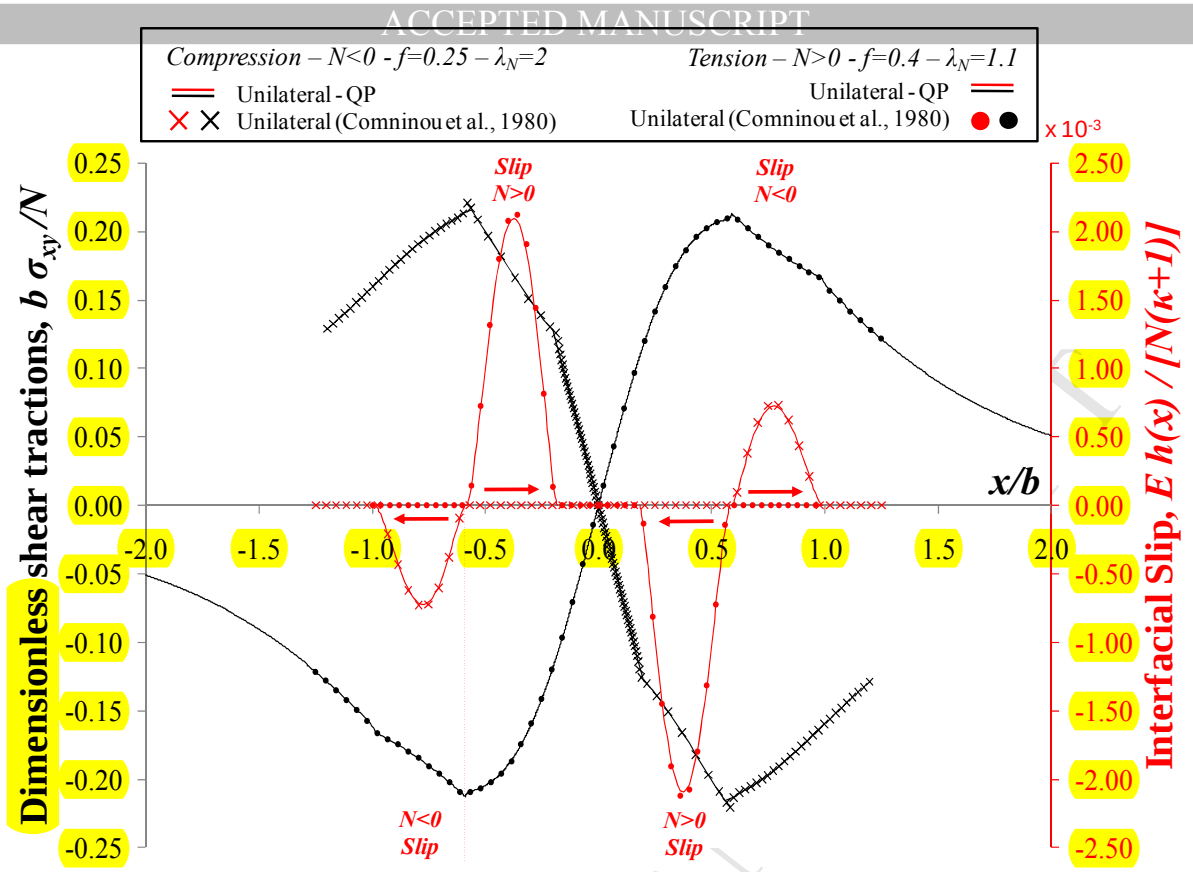

Figure 4. Shear tractions and relative displacement between layer and substrate for f=0.25, λ_N=2 (N<0) and f=0.4, λ_N =1.1 (N<0) - stationary case.

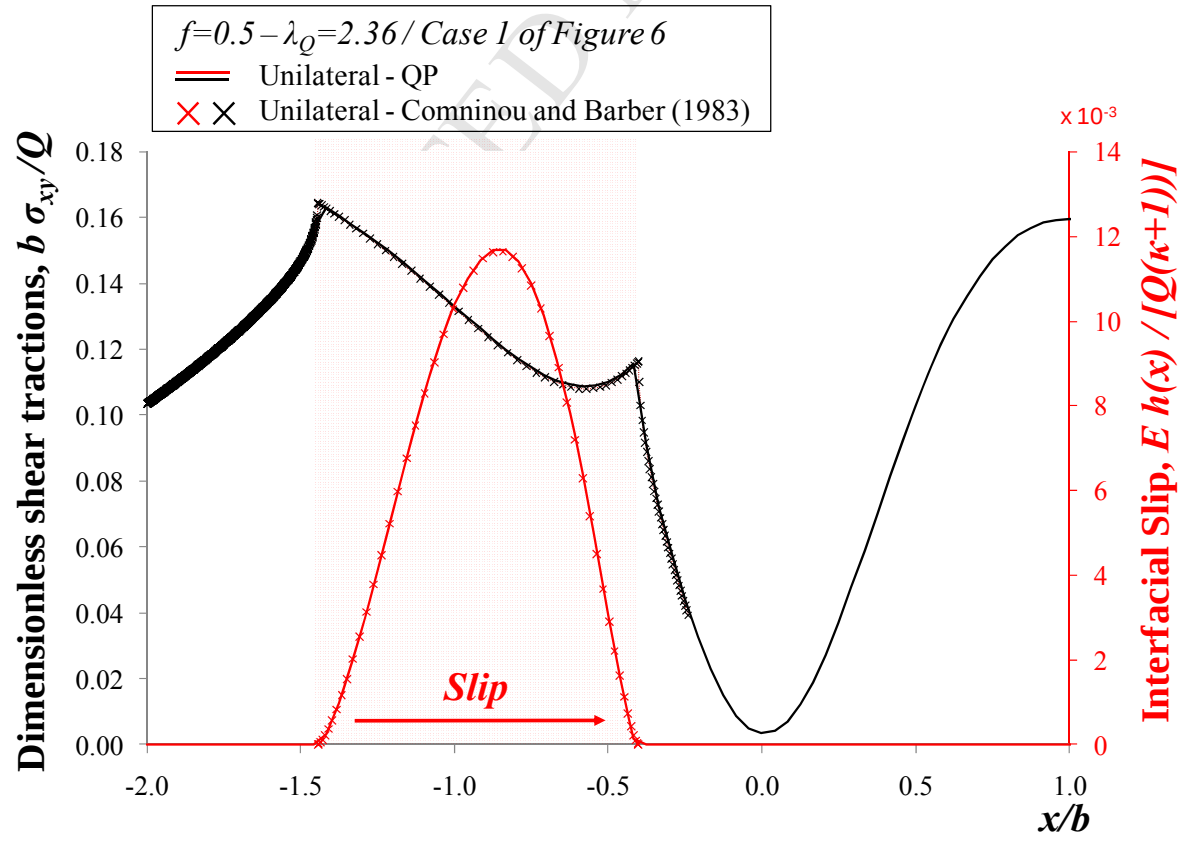

Figure 5. Shear tractions and relative displacement between layer and substrate for f=0.5, λ_Q =2.36 - stationary case.

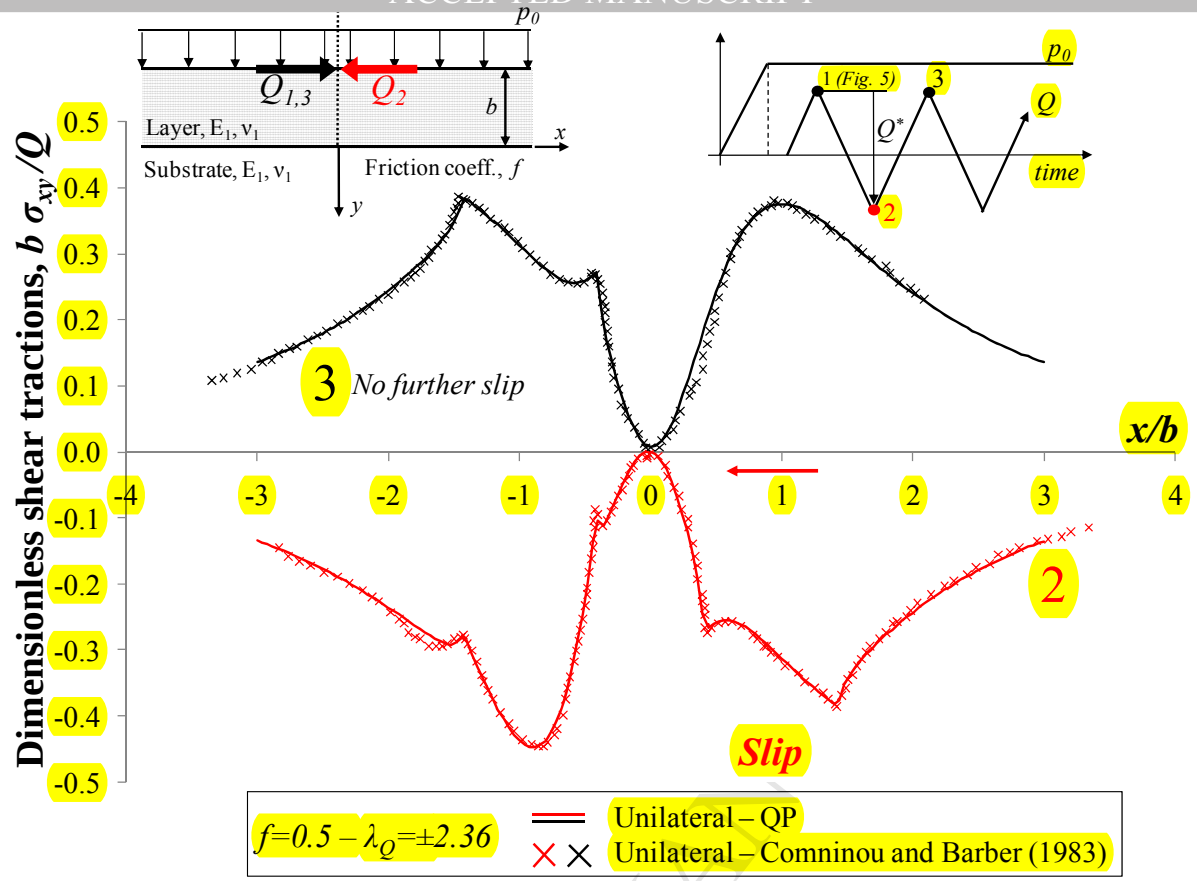

Figure 6. Shear tractions for f=0.5 and λ_Q =±2.36 (cyclic tangential load) - stationary case.

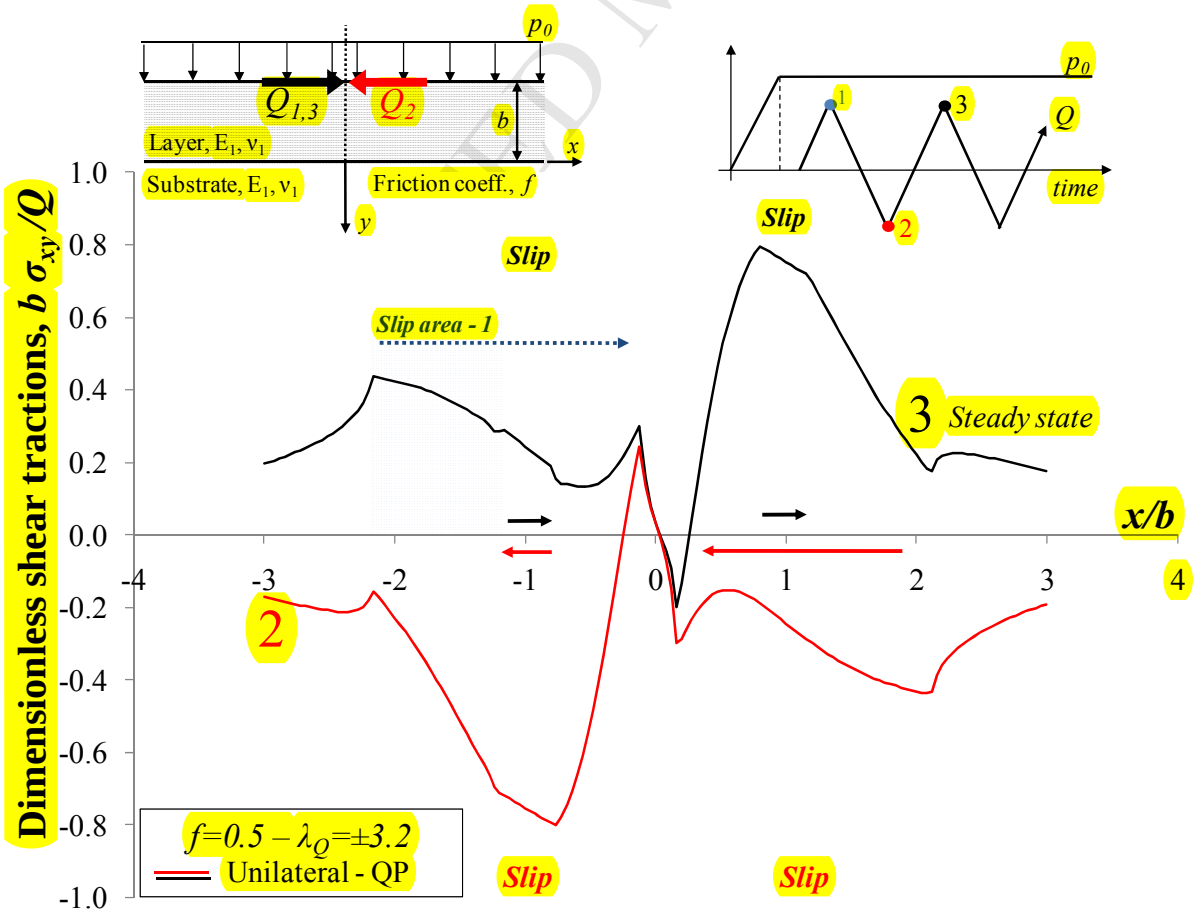

Figure 7. Shear tractions for f=0.5 and λ_Q =±3.2 (cyclic tangential load) - stationary case.

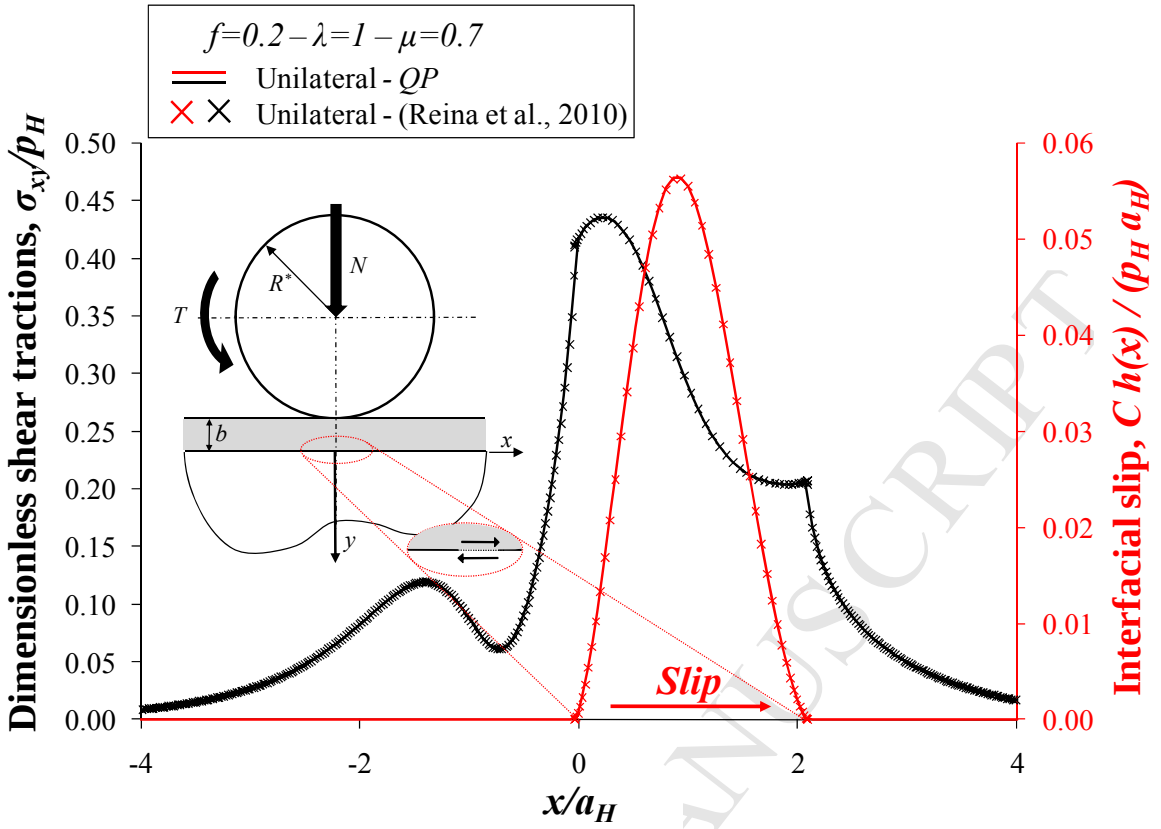

Figure 8. Shear tractions and relative displacement between layer and substrate for B=1, f=0.2, μ=0.7, λ=1 and ν=0.3 - stationary case - full sliding of a roller over the layer surface.

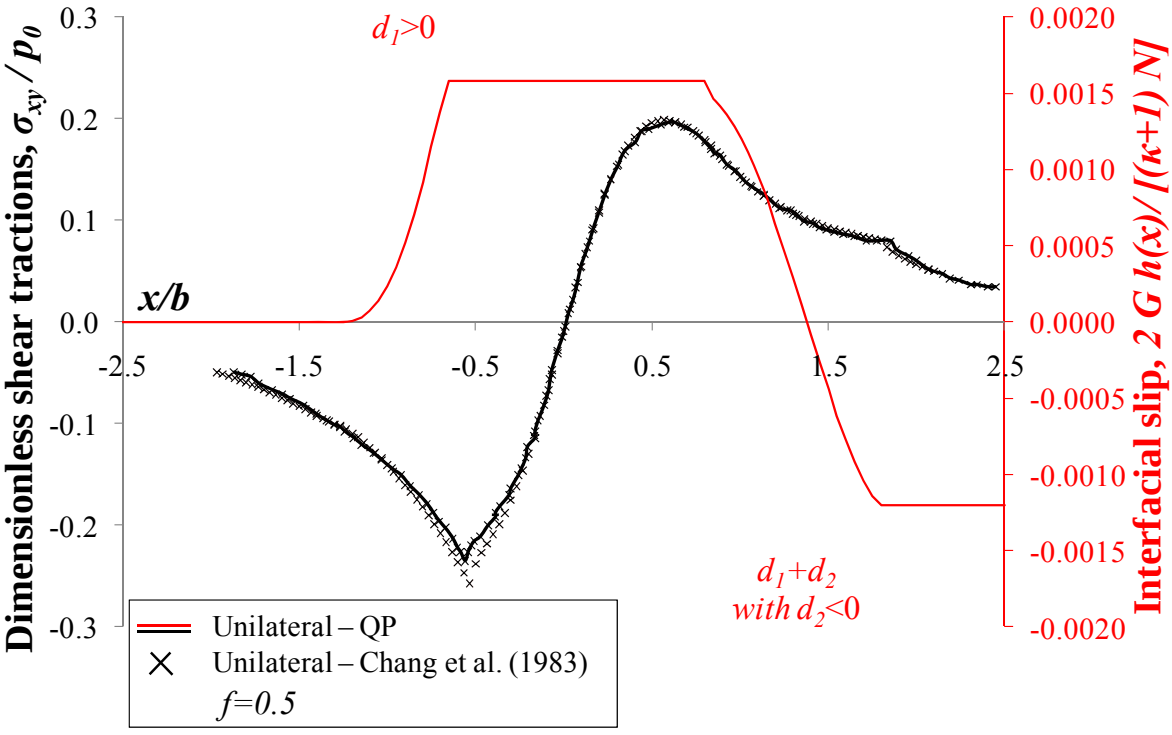

Figure 9. Shear tractions and relative net displacement between layer and substrate for λ_N =8, for f=0.5.

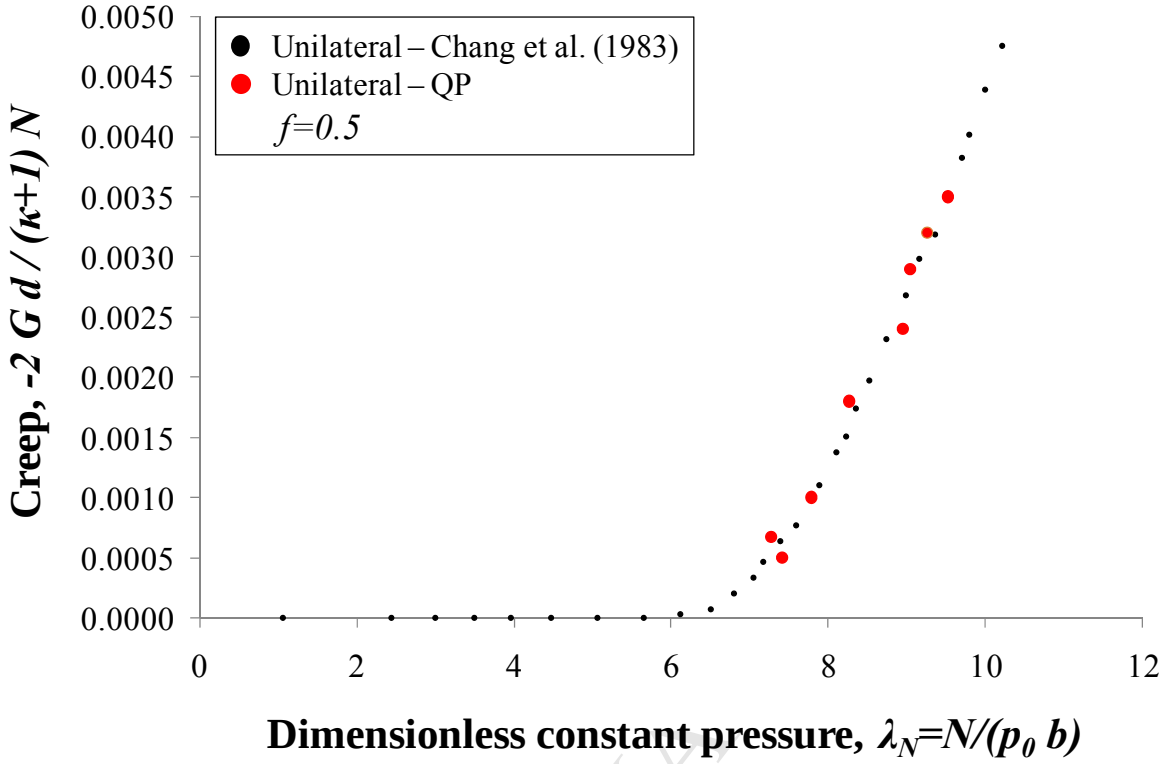

Figure 10. Relative net displacement between layer and substrate as a function of the dimensionless constant pressure, λ_N, for f=0.5.

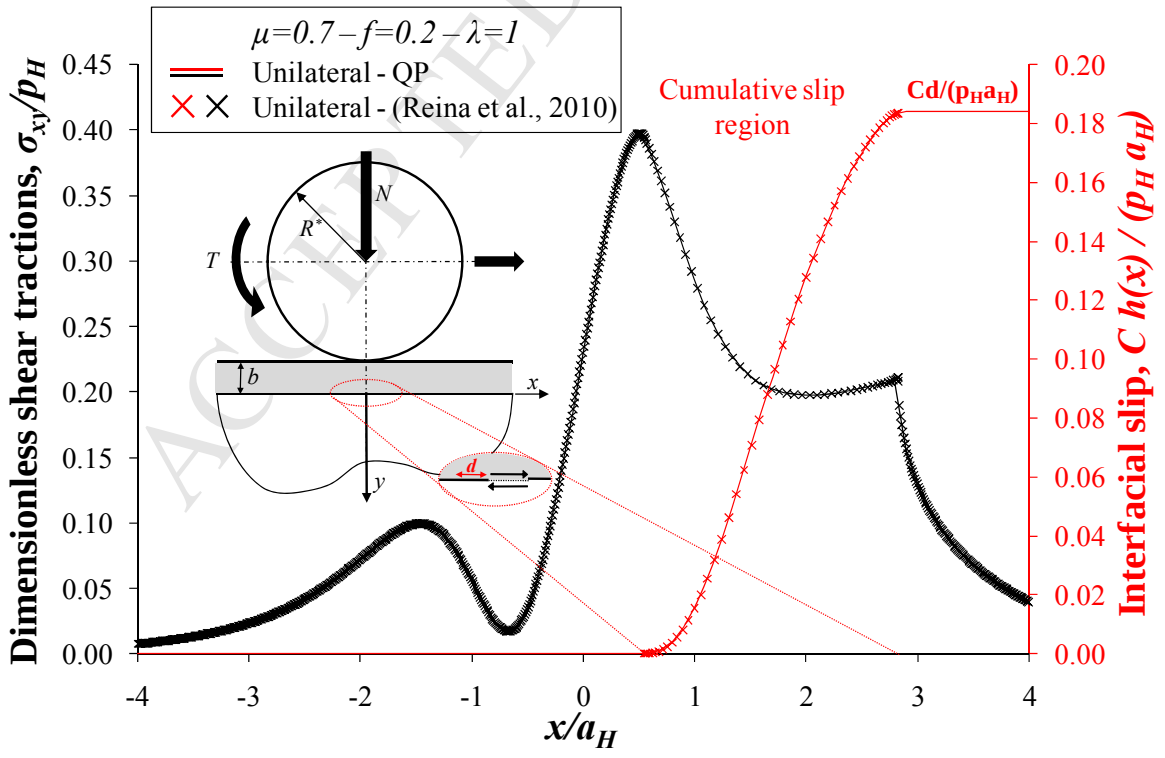

Figure 11. Shear tractions and relative net displacement between layer and substrate for B=1, f=0.2, μ=0.7, λ=1 and ν=0.3 – steady state solution for the moving load case – full sliding of a roller over the layer surface.

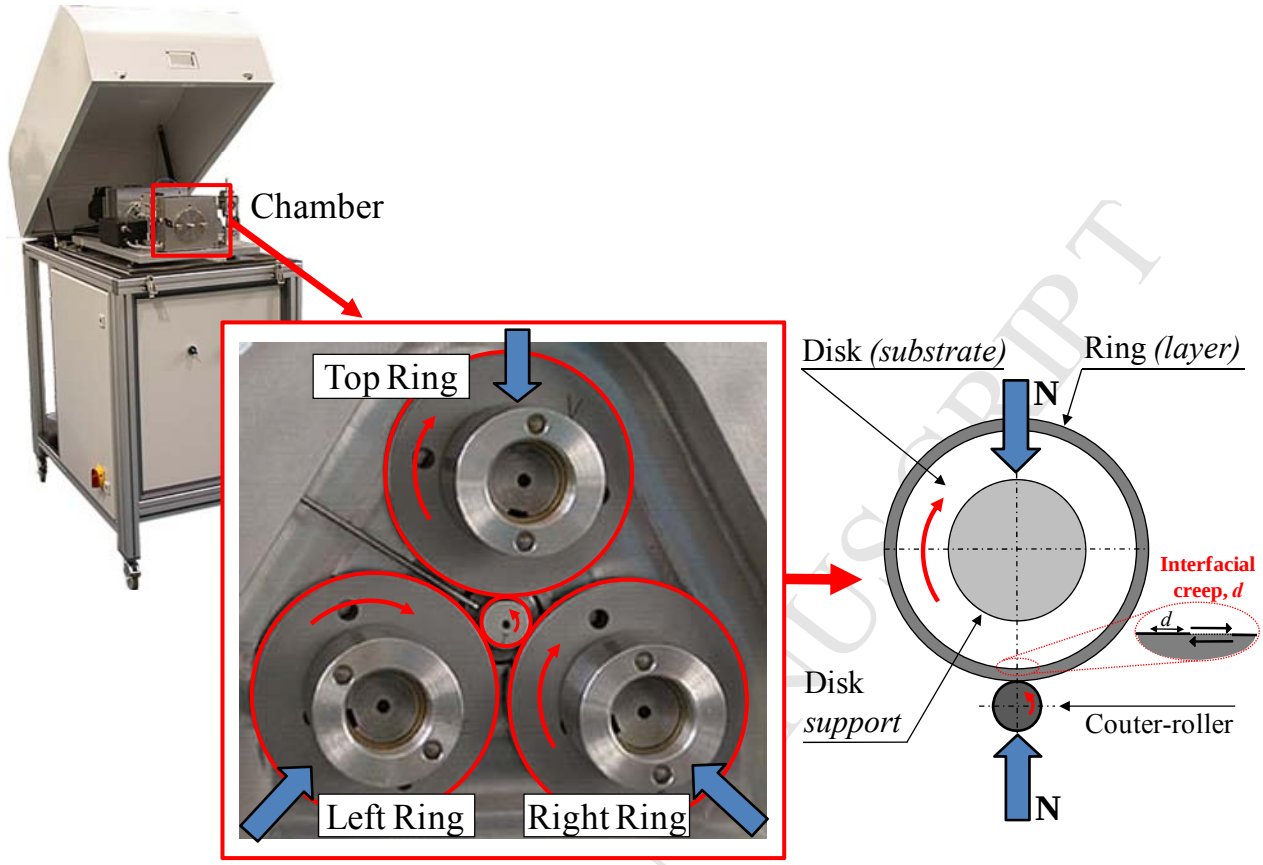

Figure 12. PCS MPR (www.pcs-instruments.com/mpr) experimental apparatus consisting of three tyred rollers and a central roller and schematic of the loading system.

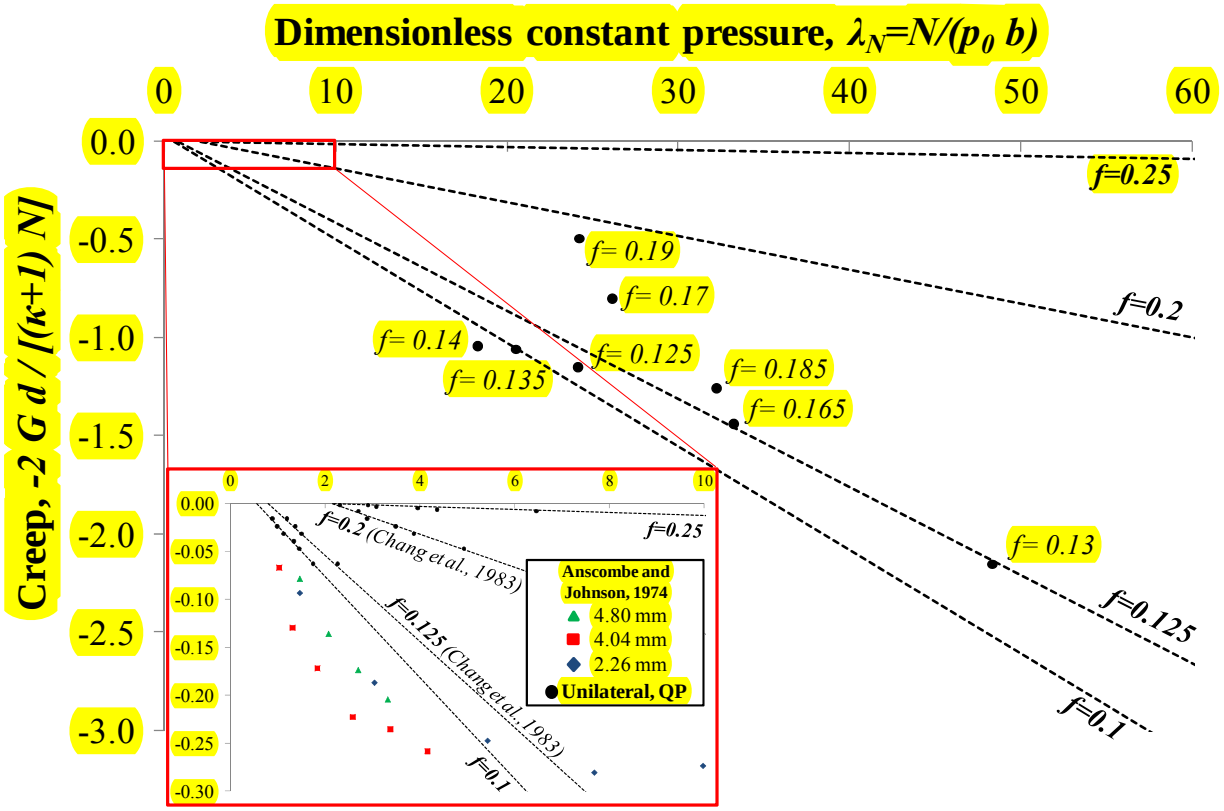

Figure 13. Net displacement, d, per revolution as a function of the dimensionless constant pressure, λ, and of the interfacial friction coefficient, f. In the same graph, comparison with experimental results and, in the inset, with Anscombe's original data (Anscombe et al., 1968 and Chang, 1983).

Notation

a	Contact semi-width
a_H	Hertzian contact semi-width
$A=a/a_H$	Dimensionless contact ratio
A_{Le}	Matrix containing the coefficient of the linear equalities of the boundary conditions to which the contact problem is subject
A_{Lie}	Matrix containing the coefficient of the linear inequalities of the boundary conditions to which the contact problem is subject
$A_{SM}=2E/\left(\pi\left(\kappa+1\right)\right)$	
$A_{DM}=2E_1\left(1-\alpha\right)/\left(\pi\left(\kappa_1+1\right)\left(1-\beta^2\right)\right)=2E_2\left(1+\alpha\right)/\left(\pi\left(\kappa_2+1\right)\left(1-\beta^2\right)\right)$	
b	Layer thickness
b_{Le}	Vector containing the known terms of the linear equalities of the boundary conditions to which the contact problem is subject
$\underline{b}_{Lie}$	Vector containing the known terms of the linear inequalities of the boundary conditions to which the contact problem is subject
$B=b/a$	Dimensionless thickness parameter
B_x	Glide dislocation density
$C=2G(1-\alpha)/\left[(k+1)\left(1-\beta^2\right)\right]$	
d	Net relative shift between layer and substrate
d_{sup}	Distance between equally spaced points at which traction, displacement and dislocation density are sampled
D_{12}, D_{22}	Kernels used to find the influence functions for a glide dislocations on the layer substrate interfacial stress field
E	Young's modulus
f	Interfacial friction coefficient between layer and substrate
$\underline{f}_{quad}$	Vector including the linear terms of the quadratic programming functional F (or F_{M})
$\tilde{F},\tilde{F}_M$	Functional of the contact problem
F_{xy}, F_{yy}	Influence functions describing the contribute to the layer/substrate shear, F_{xy}, and normal, F_{yy}, tractions, given by a triangular distribution of glide dislocation density, B_x
$\tilde{F}_{linear}$	Linear part of the functional
$\tilde{F}_{quadratic}$	Quadratic part of the functional
G	Shear modulus
G_{xy}, G_{yy}	Influence functions describing the contribute of a glide dislocation to the layer/substrate interfacial stress field
$h(x)$	Tangential shift due to distributed dislocations
$\dot{h}(x)$	First derivative in time of the tangential shift due to the distributed dislocations, $h(x)$
$h_j,h_j^{'},h_j^{''}$	Unknown tangential displacements at node j
H_{quad}	Square matrix including the quadratic terms of the quadratic programming functional F (or F_{M})
I	Identity matrix
j	Dummy variable
$\underline{l}_b$	Vector containing the lower limits of the variables contained in $\underline{x}_{quad}$
m	Trailing edge of the interfacial slip region – see (ii) in figure 1
M_1	Sub-matrix of A_{Le}
n	Leading edge of the interfacial slip region – see (ii) in figure 1
n_p	Number of points at which traction, displacement and dislocation density are sampled
N_{12},N_{22}	Kernels used to find the influence functions for a glide dislocations on the layer/substrate interfacial stress field

N	Normal load per unit depth
p_0	Interfacial uniform constant contact pressure
p_H	Hertzian pressure peak
$p(x,time)$	Surface normal stress
$q(x,time)$	Surface traction stress
Q	Tangential load per unit depth
R_a	Surface roughness
$u_{layer}(x)$	Layer tangential displacement at the layer/substrate interface
$u_{substrate}(x)$	Substrate tangential displacement at the layer/substrate interface
x	Horizontal coordinate
$\underline{x}_b$	Vector containing the upper limits of the variables contained in $\underline{x}_{quad}$
x_j	Auxiliary coordinate set used to identify the location of a point belonging to the layer/substrate interface in a fixed frame of reference (see figure 2)
$x_k=x_j/2+x_{j+1}/2$	
$\tilde{x} = x / b$	
$\underline{x}_{quad}$	Vector including the variable of the optimization process
y	Vertical coordinate
α, β	Dundurs' constants
$\zeta_j = h_j - h_{j+1}$	Difference between the tangential displacement measured at two adjacent supports
$\zeta_j^{'}, \zeta_j^{''}$	Unknown tangential displacement
$\kappa = 3 - 4\nu$	Kolosov's constant for plane strain
$\lambda_N = N / (bp_0)$	Dimensionless loading parameter
$\lambda_Q = Q / (bp_0)$	Dimensionless loading parameter
$\lambda = p_0 / (p_H)$	Dimensionless loading parameter - see figure 8 and 11 (Reina et al., 2010)
μ	Friction coefficient between disc and tyre - see figure 8 and 11 (Reina et al., 2010)
ν	Poisson's ratio
ξ	Integration variable
$\sigma_{xy}^{bil}(x,y)$	Tangential component of the layer stress field due to the bilateral solution alone
$\sigma_{yy}^{bil}(x,y)$	Normal component of the layer stress field due to the bilateral solution alone
$\sigma_{xy}^{corr}(x,y)$	Corrective component of the tangential component of the layer stress field at the layer/substrate interface
$\sigma_{yy}^{corr}(x,y)$	Corrective component of the normal component of the layer stress field at the layer/substrate interface
$\sigma_{xy}(x,y)$	Tangential component of the overall layer stress field
$\sigma_{yy}(x,y)$	Normal component of the overall layer stress field
τ	Integration variable